Finding Self-Similar and Scaling Fractal Properties in \mathbb{R} within Collatz Number Systems

Christopher C. Ladd April 4, 2025

Abstract

We further establish self-similar and scaling fractal properties in the space of real numbers $\mathbb R$ by inverting the principles of the Collatz function to create a directed acyclic graph (DAG) framed in the form of a rooted tree to measure these behaviors. Here, focus pivots from conjectural intents of the Collatz problem to study the system's generative, non-linear aspects. Analogous ancestry is used to compare sibling nodes' progressive lineage defined as their respective sub-tree node count. The study begins with a notable disproportional lineage at the first branching point of the tree. We extend this analysis to six additional pairs to confirm invariant, power-law scaling behavior within the tree's hierarchical structure by visually observing self-similar patterns and by calculating fractal dimensions and Hurst Exponents using log-log analysis. From this, a novel instance of scaled fractality emerges in a deterministic number system, fully contained in $\mathbb R$.

Keywords: self-similar, fractal, scaling fractal, fractal dimension, power law, box counting, Hurst Exponent, rescaling, R/S, maximum lag, Collatz Conjecture, Collatz function

1 Introduction

Complexity and fractals have gained notice this past century. Once termed "monsters" as Mandelbrot recounts in *The Fractal Geometry of Nature* (p. 4, 9) [9], their foundations have been furthered established in various aspects of math and science. They are embedded in natural systems, integral in computational theories, like Wolfram's *A New Kind of Science* [17], and even found at the heart of The Clay Institute's Riemann Hypothesis million-dollar question [7].

Focusing on number theory, these concepts are firmly established in the complex plane \mathbb{C} and connect with the real number system \mathbb{R} in many ways, almost always through intended design. Though those monster-adjacent may argue such constructs are scripts expressing a play acted upon an unseen stage and backdrop. Yet finding fractal structure emerging naturally absent intent or reliance upon complex numbers is uncommon.

But such could be possibly less so, perhaps waiting for further evolution of a vocabulary to be described. The topic is exemplified outside formal academic literature in an online mathematical forum: a user questions whether self-similar visuals constructed from OEIS sequence A001511 [13] imply fractal behavior and associated complexity. An apt, first reply follows: 'How do you define it...' [18].

Aware of this gap, Mandelbrot provided a new term, *scaling fractal*, where the adjective (possibly implying a form of order) mitigates the noun (potentially denoting pure chaos) (p. 18) [9]. It is in this spirit we 1) provide a firm example of fractional complexity in the real number system and 2) offer data and observations to help navigate this gray area. All of this is facilitated by the Collatz Conjecture.

The conjecture is one of the most studied number systems in mathematics. In 1937, Lothar Collatz propositioned a faultless map to 1 for any natural number $n \in \mathbb{Z}^+$ by repeating: halve n if it is even; otherwise, triple it, then add 1. Still unresolved [8] and possibly unprovable [5], the problem's potential unassailability could be described monster-ish itself.

The system's fractal properties in \mathbb{C} have been established in academic literature [12, 6, 15, 16]. However, within the domain of \mathbb{R} , self-similar qualities are observable [4], as well as persistent power-scaling properties [3]. We add to this niche intersection where Collatz dynamics again demonstrate this form of structured complexity in what is considered real.

2 Methodology

2.1 Definitions and Terminology

We focus on a perspective outside the conjecture's proof. Probabilities and cycles are exempt by definition. Determinism creates one path to reach 1 and then halts. We specifically employ the "Collatz function" C(x) and not the "3x + 1 function" T(x) as distinguished by Lagarias (2012, p. 1) [8].

Here, using the *Collatz function* above, we define and express it as:

For
$$n \in \mathbb{Z}^+$$
, $C(n) = \begin{cases} f(n) = \frac{n}{2}, & \text{if } n \equiv 0 \pmod{2}, \\ g(n) = 3n + 1, & \text{if } n \equiv 1 \pmod{2}. \end{cases}$

Mandelbrot's framework for fractals provides a reference point of formal definitions [9]. Except for *Analogous Ancestry*, *Lineage*, and *Sibling Lineage*, tree-oriented terms were adapted from Cormen et al [2].

- (Scaling) Fractal: A geometric object in Euclidean space \mathbb{R}^E characterized by fractal dimension D strictly exceeding its topological dimension D_T , exhibiting self-similarity and scaling.
- Self-Similar: A structure that maintains consistent patterns across multiple scales.
- Scaling: A property where structural relationships remain invariant under transformation.
- Node: An integer value mapped into the directed tree via C^{-1} .
- Lineage: The total count of descendant nodes in a sub-tree plus the node itself.

- Analogous ancestry: An extensible, comparative framework for analyzing hierarchical relationships.
- Sibling lineage: The proportional lineage within a sibling pair.

2.2 Method

With C(n) we create rules of its inverse $C^{-1}(x)$ to construct a directed tree graph starting at Node 1 and iterating to infinity. To invert C(n), exchange dependent and independent variables, then solve for the new dependent variable. We ensure the partitioned domains of C(n) are reflected in the co-domains of $C^{-1}(x)$. This results in the following (with one added exception):

For $x \in \mathbb{Z}^+$,

$$C^{-1}(x) = \begin{cases} f^{-1}(x) = 2x, \\ g^{-1}(x) = \frac{x-1}{3}, & \text{if } x \equiv 1 \pmod{2} \quad \text{and } x \in \{6m+4 \mid m \in \mathbb{Z}_{\geq 0}\}, \quad \text{except } g^{-1}(4) \to 1. \end{cases}$$

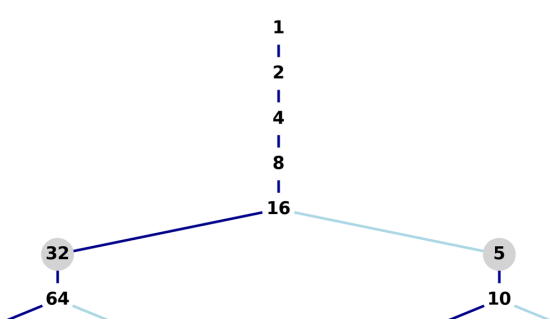
We note:

- $g^{-1}(x)$ is constrained to produce only odd numbers, while $f^{-1}(x)$ innately produces only evens.
- $C^{-1}(x)$ cannot produce an iterate with equal numbers and thus strictly implies only one calculation by $C^{-1}(x)$ can produce any number. This results in unique paths.
- All nodes are *parent nodes*, producing either one even-numbered *child node* or a pair of even and odd (*sibling*) children. Thus, it must have a least one or possibly two *egress edges* to its children.
- A node cannot be its own parent.
- A node has only one *ingress* from its parent (except the root node).

The resulting structure is not novel, recreated anew for various purposes. For example, it is currently visible on Wikipedia's Collatz Conjecture page to represent a bottoms-up approach towards a proof [1]. At OEIS, A122824 is an instance described as triangle numbers to the Collatz problem [10]. It was derived to study Mersenne primes and create faster code towards the conjecture's proof [11].

Figure 1 shows the first branching at Node 16 in level 4 to create siblings N5 and N32 for level 5. Past here all return paths must utilize one of these siblings. The study begins here and after descends to six additional pairs shown in the continued tree graph found in the Results section. Please note: The rooted, (directed) tree graph represents both C(n) (going up) and $C^{-1}(x)$ (going down); however, contextually not at the same time. Direction is assumed understood, so edges are visualized without arrows.

Figure 1: Top-down, rooted tree graph after six iterations from Node 1 (level 0). Dark blue edge colors indicate $f^{-1}(x)$ and light blue edges indicate $g^{-1}(x)$. The highlighted gray nodes in both figures are included in this analysis.



2.3 Analogous Ancestry

After tree construction, we then in sequential order apply C(n) to numbers n=1 to 10^7 . We track the complete sequence of ancestor nodes transversed. After each number completes this process, data increments for impacted ancestors, and then all calculations are updated. This sequencing serves as the domain of independent variability for event and time basis in this study.

Analogous ancestry intends to be a set of tools to study C(n) and $C^{-1}(x)$. For now, it collects lineage data of sibling pairs. We note lineage is a conserved quantity, and so, comparisons of lineage groupings are inherently proportional.

Potential additional tools, such as *level lineage* and *odd density* are under review. Deeper discussion can be found in Appendix A.1.1.

2.4 Visualization Analysis

Scatter plots help visually identify self-similarity and fractal behaviors. Specific examples N5, N80, N85, and N320 are highlighted in the results.

Given the basis of conserved quantity, a sibling node's data equals or mirrors its counterpart as shown in Figure 2. Given such, we present only one of the pair as needed for brevity. All pattern data is found in Appendix A.2.1.

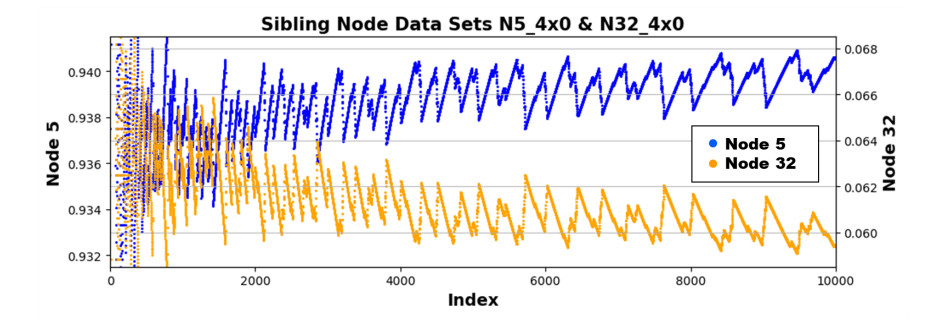


Figure 2: Pattern sample from proportional lineage data for siblings N5 and N32. It is the full set of the fastest sampling rate from the smallest range.

2.5 Data Set Definition

Proportional sibling lineage data was collected for four data sets per node, sampled at increasing factors of 10 (1, 10, 100, 1000). 10,000 elements per set was partly informed from a preliminary examination of the Hurst exponent calculation method. These findings added to the preference for a basic design, which was was employed to reduce possible external factors and increase visibility for properties tested. Table 1 details:

Sampled Range (1 to)	Sampling Rate (every nth element)	Reference Name
$10,000 (10^4)$	$1 (10^0)$	N5_4x0
$100,000 (10^5)$	$10(10^1)$	$N5_{5x1}$
$1,000,000 (10^6)$	$100 \ (10^2)$	$N5_6x2$
$10,000,000 (10^7)$	$1,000 (10^3)$	$N5_7x3$

Table 1: Data collection range, sampling rate, and nomenclature. The left and middle columns translate to conditionals used in the code to regulate set size. Reference Name reads: "Node Number _ Sampled Range by (x) Sampling Rate" (in terms of base-10 order of magnitude).

2.6 Data Set Code

The N5-N32 example below is illustrative of the general code ¹. A list index method, where node number equals the index, tracks lineage. The code is preset to bypass levels 0-4. This preset and division-by-zero exclusion cause datasets to nominally vary under 10,000 in size. Actual set sizes can be referenced in Table 6.

```
%%% Variables %%%
fiveOr32 = ([0]*33)
                      % Lineage index list
fiveOr32[5] = 11
                      % Preset
N5_{x}, N32_{x} = [] , []
%%% Function Definition %%%
def find_And_Set_Ancestor_Path(number):
    path=[number]
    while number != 1:
        if number % 2 == 0:
            number = number // 2
        else:
            number = (3 * number) + 1
        path.append(number)
    path.reverse()
    if len(path) >= 5:
        fiveOr32[path[5]] += 1
    return
```

 $^{^{1}} Code \quad and \quad dataset \quad available \quad at \quad \text{https://github.com/claddblog/CollatzRealScaleFractals.}$

```
%%% Main Code %%%
for n in range(17,10000001):
    find_And_Set_Ancestor_Path(n)

%%% Conditionals %%%
    if (x % 10^[0... 3] == 0) and (x <= [10^[3... 7]) and (sum(fiveOr32) != 0):
        N5_'x'.append(fiveOr32[5]/sum(fiveOr32))
        N32_'x'.append(fiveOr32[32]/sum(fiveOr32))</pre>
```

Path lists of the first sixteen numbers are below to help visualize data collection and motivation for the code preset.

```
N: [1, ...Reversed Path Sequence..., n]
1: [1]
2:
    [1,2]
   [1,2,4,8,16,5,10,3]
3:
4:
   [1,2,4]
5:
   [1,2,4,8,16,5]
    [1,2,4,8,16,5,10,3,6]
    [1,2,4,8,16,5,10,20,40,13,26,52,17,34,11,22,7]
8:
    [1,2,4,8]
9:
    [1,2,4,8,16,5,10,20,40,13,26,52,17,34,11,22,7,14,28,9]
10: [1,2,4,8,16,5,10]
11: [1,2,4,8,16,5,10,20,40,13,26,52,17,34,11]
12: [1,2,4,8,16,5,10,3,6,12]
13: [1,2,4,8,16,5,10,20,40,13]
14: [1,2,4,8,16,5,10,20,40,13,26,52,17,34,11,22,7,14]
15: [1,2,4,8,16,5,10,20,40,80,160,53,106,35,70,23,46,15]
16: [1,2,4,8,16]
```

2.7 Empirical Analysis

The methodology designed intended a smaller group of well-established indicators for this study. Indeed, other methods, such as Recurrence Qualification Analysis, wavelet transforms, and FFT analysis would contribute. Box-counting for D and rescaling for H were selected due to early results indicating both as separate, strong indicators.

Historically and generally they are used in complementary fashion; the fractal dimension is thought of as a local indicator, the Hurst component as global. Both are related by the equation H+D=2 from which one is often derived from the other. This was not the case here. Both were estimated from different log-log scaling methods and without assuming any level of interdependence (this does not mean they are not correlated to some degree). Both were examined at a high level for details towards final application. These details are explained in their respective sections.

2.7.1 Fractal Dimension Estimation and Data Preparation

The log-log scaling box-counting method involves dividing the data range N into progressively smaller intervals ("boxes") and counting the number of non-empty boxes. The relationship between box size ϵ and box count $N(\epsilon)$ is expected to follow a power-law behavior:

$$D = \lim_{\epsilon \to 0} \frac{\log N(\epsilon)}{\log(1/\epsilon)}$$

By taking the logarithm of both sides, the relationship becomes linear. The slope is computed using least-squares method and signifies the fractal dimension:

$$\log(N(\epsilon)) = D \cdot \log(1/\epsilon) + C$$

Results could vary significantly depending on methods used. We explored and evaluated options for normalization, box sequence, and box scaling aspects to gauge output validity.

Data was normalized before estimating D. Min/max and Z-score methods were explored. Both produced essentially the same results. We selected Z-score for its high level of application as a standard. Equations for both methods:

$$X_{\rm Min/Max\ norm} = \frac{X - X_{\rm min}}{X_{\rm max} - X_{\rm min}}$$

$$X_{\text{Z-Score norm}} = \frac{X - X_{mean}}{X_{std}}$$

Regarding sequence and scale, we selected three nodes (N5, N85, N320) of varying analogous ancestry in sibling lineage and level. The two most opposing sample rates, 4x0 and 7x3, were bookends to range our evaluation. Three sequence types were examined (geometric, exponential, pseudo-linear) across three scales (9, 11, 13). Fractal dimension D was calculated for all combinations (described in the below table) including normalization methods.

Table 2: Box sequence and scaling repeated for both normalization methods $(i \ge 0, j \ge 1)$.

Sequence Type	Scale 9	11	13
Geometric: 2^i	[1, 2, 4, 8, 16, 32, 64, 128, 256,	512, 1024,	2048, 4096]
Exponential $\lfloor j^{\pi} \rfloor$	[1, 8, 31, 77, 156, 278, 451, 687, 995,	1385, 1869,	2456, 3159
Pseudo-Linear	[1, 2, 5, 10, 15, 20, 35, 55, 75,	105, 135,	190, 205]

Overall the results were effectively the same. Data can be found in Appendix A.3. The geometric sequence using scale of 11 was selected for its intrinsic power-scaling and heuristic significance. We note the same conclusions would be arrived at using any combination above.

2.7.2 Hurst Exponent Estimation and Analysis Preparation

The Hurst exponent (H) was computed using the rescaling method (R/S) to quantify long-term memory and persistence across data sets. It does this by examining the time series decrease in auto-correlations against longer periods or lagging periods of time by splitting the time series into equal, non-overlapping segments where the logarithm is taken of the range of cumulative differences from the mean (R) divided by the standard deviation of the segment (S). This is plotted against the logarithm of the size of the segment. The slope is computed using least-squares method and signifies H.

For data set size, various intervals of contiguous block sizes for N5 (1000, 2000, 5000, 10000, 25000, 50000) within n=1 to 10^6 were examined. For maximum lag, we studied several segment lengths (50, 100, 250, 500) across all node by data sets. For reasons between converging stability and optimal parameterization, data set size of 10,000 and maximum lag of 100 were selected. Details are found in Appendix A.4.

The definition used here:

$$H = \lim_{s \to \infty} \frac{\log(R/S)}{\log(s)},$$

Where R is the range of cumulative deviations from the mean, S is the standard deviation, and s is the segment size. Data normalization is considered part of the Rescaled Range (R/S) calculation.

H values:

- $H \approx 0.5$ suggests a random process.
- H < 0.5 indicates mean-reverting behavior.
- $\bullet~H>0.5$ implies persistence and long-range dependence.

3 Results

Opening Note: Although there were interesting point results in the preliminary analysis from here and through the Conclusion section, references to fractal dimension and Hurst exponent only regard the parameters defined and decided upon in the Methodology section: Data Sets as detailed in Section 2.5, D calculated using Z-Score normalization with the geometric box sequence $2^i, i \in [0, 10]$, and H with a maximum lag of 100.

3.1 Summary Lineage Data

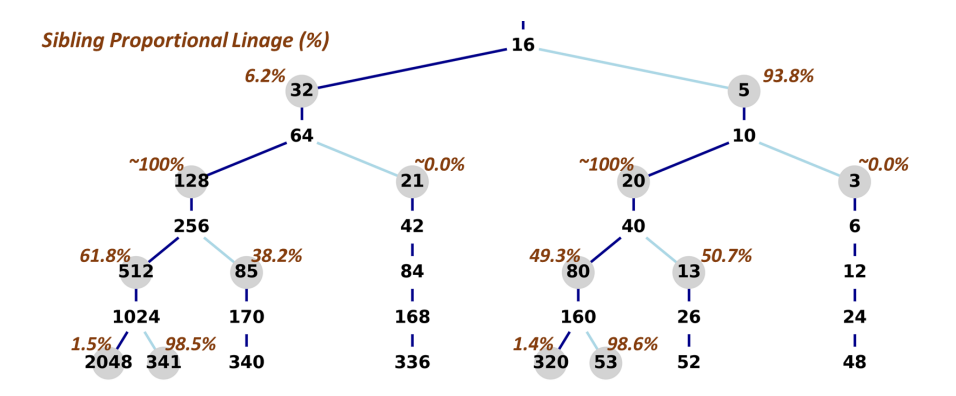


Figure 3: Continuation of tree structure from Figure 1. Sibling lineage percentages are found on the upper-outside corners of the sibling pairs. Lineage table data can be found here in Table 5.

3.2 Summary Log-Log Analysis Data

Note on removed table²

Table 3: Highlighted Basic Statistics: Noting H + D = 1.953

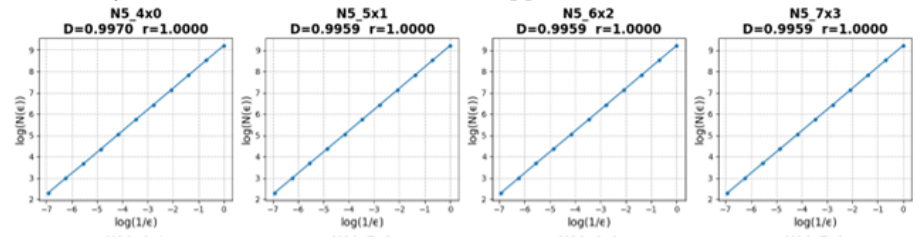
Metric	Hurst Exp. (H)	R-Value	Fractal Dimension (D)	R-Value
Mean	0.9572	_	0.9960	-
Stnd. Dev.	0.0305	_	4.52×10^{-4}	_
Median	0.9659	0.9998	0.9659	1.000
Minimum	0.8990	0.9748	0.9949	1.000
Maximum	0.9950	0.9999	0.9970	1.000

 $^{^2}$ An earlier correlation data table was removed due to inconsistency across revisions. In addition to correlations among log-log methods (D and H) exhibiting high sensitivity, relationships between fractal dimension and associated fit metrics (e.g., R-values) also varied significantly with data preparation and scale parameters.

Table 4: Annotated Log-Log Linear Regression Data, highlighting 4x0 and 7x3 data sets for selected nodes N5, N80, N85, and N320, from levels 5, 9, and 11. All data can be found in Appendix A.1.2.

Data Set	H	R-Value	P-Value	$\mid D$	R-Value	P-Value
N5_4x0 N5_7x3	0.9810 0.9611	0.9998 0.9998	$\begin{array}{c} 2.18 \text{x} 10^{-167} \\ 5.12 \text{x} 10^{-167} \end{array}$	0.9970 0.9959	1.000 1.000	$1.25 \times 10^{-23} 2.39 \times 10^{-25}$
N80_4x0 N80_7x3	0.9763 0.9476	0.9997 0.9998	$1.86 \times 10^{-157} 2.07 \times 10^{-161}$	0.9970 0.9959	1.000 1.000	$1.25 \times 10^{-23} 2.39 \times 10^{-25}$
N85_4x0 N85_7x3	0.9093 0.9096	0.9825 0.9996	$7.80 \times 10^{-72} $ 1.38×10^{-150}	0.9959 0.9959	1.000 1.000	$7.85 \times 10^{-24} 2.39 \times 10^{-25}$
N320_4x0 N320_7x3	0.9858 0.9577	0.9998 0.9998	$9.63x10^{-162} 5.10x10^{-168}$	0.9969 0.9959	1.000 1.000	$1.13x10^{-23} 2.39x10^{-25}$

Figure 4: Box Counting Log-Log Plots for Node 5. All node plot visuals are essentially the same and can be found in Appendix A.3.



3.3 Visualization Analysis

3.3.1 Scatter Plots

Nodes N5, N80, N85, and N320 are highlighted for cross-level and varying pattern details. The nodes have all four data sets overlaid. To conserve graphic space, data set coloring is standardize: 4x0 - Blue, 5x1 - Orange, 6x2 - Green, 7x3 - Red.

Two graphics are shown for each node to show relative alignment across data sets, while noting no x-axis data adjustments were made to achieve this. The top graphic spans the entirety of data sets (1 to 10K), and the bottom displays the last 30% (7K to 10K). This is intended to show a top level view and an underscoring of the progression.

For all, the y-axis boundaries are set to the minimum and maximum values of the last 80% of the upper visual and last 30% of the one or two below it; this allows better pattern expression. All individual scatter plots can be found in Appendix A.2.1.

The following commentary is far from exhaustive, yet covers the objectives of addressing the potential behaviors studied and acting as working examples of the methodology.

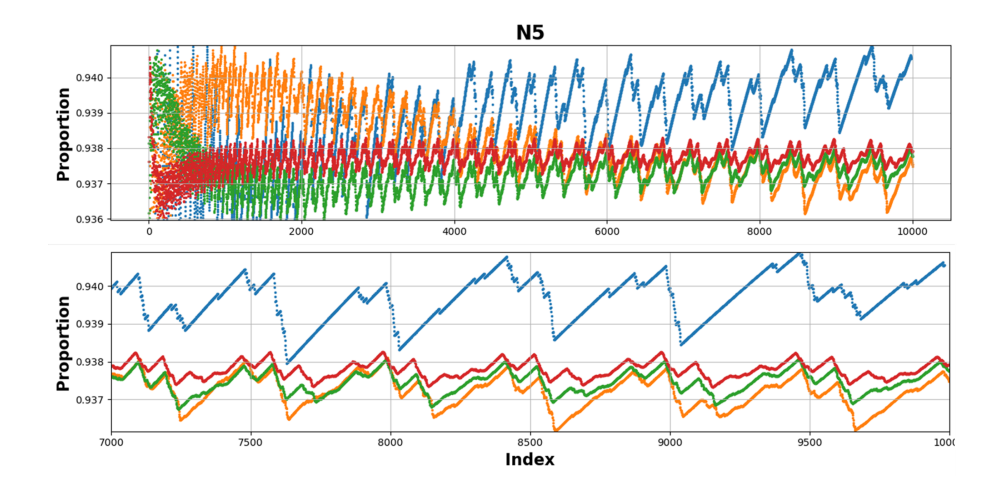


Figure 5: Node 5, Level 5. Clear similarity in patterns across datasets are seen in the lower plot. In the upper plot, the 4x0 (blue) data set seems to have lengthening periods of patterns. This seems matched in the lower plots by the other data sets with synchronous behavior. Comparative frequency assessment across data sets could provide further insights.

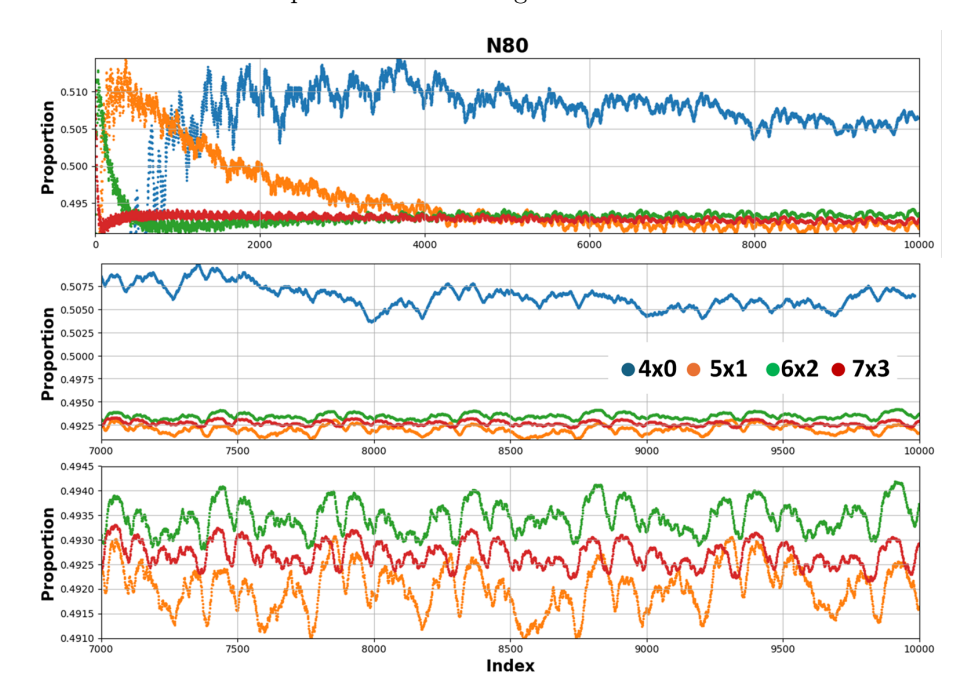


Figure 6: Node 80, Level 9. Here the lower graphic has two versions as the 4x0 (blue) data set's difference somewhat mutes the other three wave forms; however, the 5x1 (orange) dataset depicts a quick pivot to align (upper graphic between index 1 to 2000). This rate of change (retention of large values and quick pivoting to converge) is different and may depict a distinction among patterns and behaviors. Also the breakout shows "converging" becoming distinct at a range of 10,000ths.

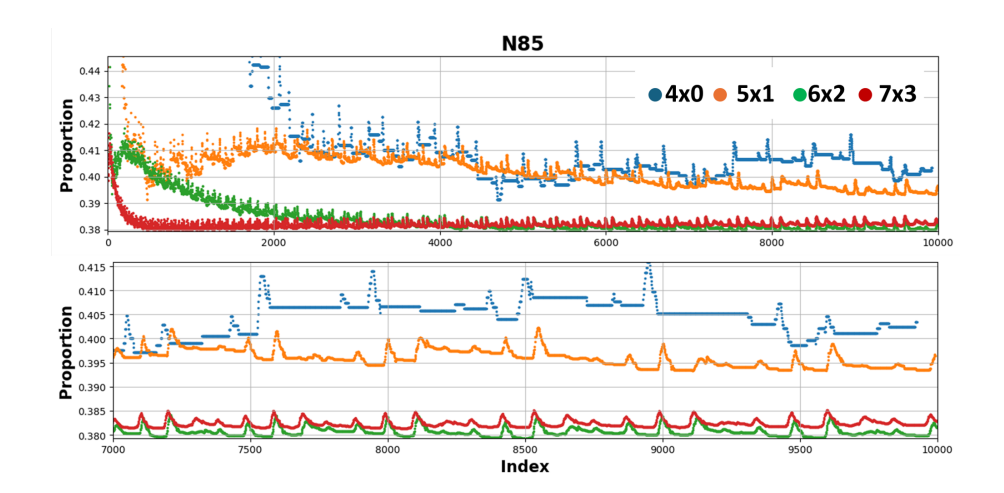


Figure 7: Node 85, Level 9. As the only descendant highlighted from N32, its sibling lineage 38.2% is comparatively higher to others, while its cumulative lineage is 2.4%. The peaks in its patterns are distinct. Similar to N80, there is a sharp pivot to converge but in data set 6x2 (green). This is contrasted to the other nodes converging faster overall.

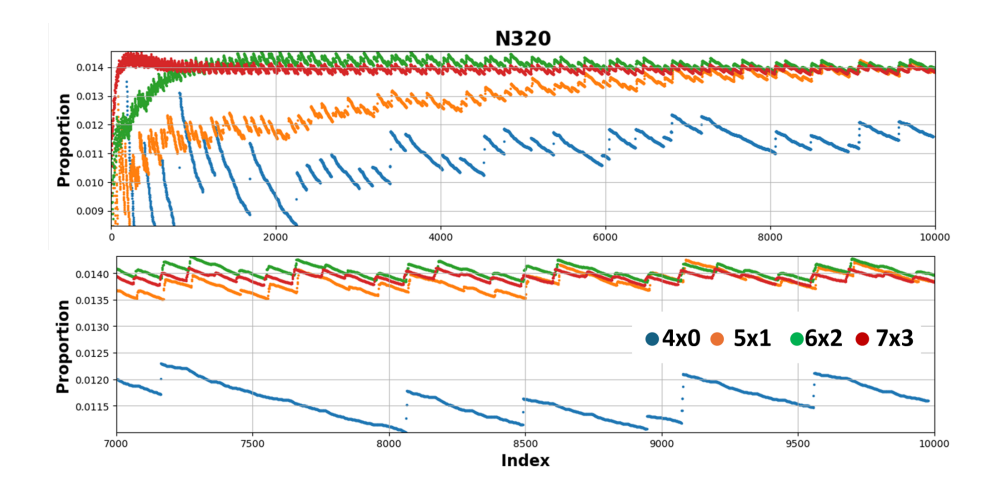


Figure 8: Node 320, Level 11. Its sibling lineage at 1.4% is comparatively low yet the patterns remain prominent and distinct compared to other nodes in comparable linage scenarios, like those in level 7 (see Figure 10). Arguably, it has the most uniformity in shape considering angles and straight lines.

4 Key Observations

- Regarding *D* and *H* data output, the fractal dimension values come close to 1.0 at times while not reaching it. The consistency reinforces a nearperfect fractal self-similarity across multiple scales.
- D and H obey the linear relationship of time-series self-affine models: $D + H \approx 2$ with a value of 1.9853.
- The persistent R-values with median values of 0.9998 (H) to 1.0 (D) indicate a highly structured log-log relationship, suggesting that the observed power-law behaviors are intrinsic to the system rather than random artifacts.
- With few exceptions, the Hurst exponent is > 0.9 throughout, showing high degree of memory in the system.
- The sensitivity and considerable change to correlation values observed in initial testing for box sizes and the Hurst exponent engenders skepticism to apply correlation analysis across methods, like Pearson values in analyzing H and D^3 .
- Close-to-zero P-Values for much of data demonstrate clear statistical significance, supporting scale-invariant properties.
- For the Hurst exponent extended analysis for maximum lag by node data set (see Appendix A.4.2), a somewhat similar pattern is seen for sibling node pairs N13-N80 and N53-N320, both descendants of N5.
- Regarding the visual graphics of the four selected nodes, periodic patterns for node pairs are visible and seemingly distinct.
- The visual of rooted tree graph itself can be considered a fractal form. As iterations persist, the known growth behavior will carry forward.
- As sampling rates scale, patterns trend to converge in value and decrease in amplitude. For most nodes, this is exhibited for the 5x1 (orange) data set in its increasing proximity to 6x2 (green) and 7x3 (red) data.
- The bottom visuals show data sets 6x2 (green) and 7x3 (red) seemingly converging to proximate proportional values.
- While not always perfectly synchronous, a notable portion of patterns' oscillatory behavior is in alignment. This implies a substantial degree of self-organization within the system.
- In this aspect of synchronicity, all data sets seem to extend in length of periodicity.

 $^{^3}$ This ultimately extended to within methods.

5 Discussion

Using datasets spanning multiple orders of magnitude within a hierarchical system to notable depth, we confirm that self-similar and scaling fractal properties hold across all sampling scales for the Collatz-inspired systems, demonstrating their fundamental role in the system's structure within \mathbb{R} . This further expands their definition and relevance beyond complex systems.

Considering data sets sampling rates and maximum lag values, the similar patterns of Hurst exponents for descendants of N5 conveys an interesting persistence that appears more stable compared to other nodes. Given these nodes inherit the most lineage, this continues establishing the system's scaling behavior and acts as a working example of what analogous ancestry was created to do.

Earlier before the above results, the consistent near-1.0 fractal dimension was considered most likely only a strong linear scaling behavior with fractal-like properties. This was combined with understandable misconceptions of fractal dimensions inability to be an integer value. Still, the near-unitary value suggests a more constrained form of self-similarity beyond pure recursive fractal growth.

This is considered with observing complex behavior rising from natural numbers based on two simple rules regarding even and odd properties involving the keystone primes 2 and 3. Such complexity from simple rules is a hallmark of fractal behavior and complex systems.

These findings raise questions about the fundamental nature of iterative number systems and linearity, particularly given the exact input of sequential counting numbers effected a known non-linear system to express further unknown non-linear characteristics.

The presence of power-law scaling within Collatz-like systems in \mathbb{R} may suggest such structuring is more common in discrete mathematics than previously assumed.

5.1 Interpretation of Results

The dataset exhibits extremely strong fractal self-similarity across all scales. The power-law scaling is nearly perfect (R = 1.0000, slope 0.996). This is joined with almost no statistical uncertainty (extremely low P-values).

The resulting, unintended summation of the means of H + D = 1.953 provides further validation of the behaviors tested for.

The system is highly structured, deterministic, and follows hierarchical self-organization. Long-range correlations (Hurst >0.90) confirm that the structure persists across time and scale.

The presence of self-similarity across scatter plots compels. Data sets show a high degree of synchronicity across scaling of nodes. This includes other scale-invariant properties, like patterns, proximal value convergence, and oscillatory behavior.

5.2 Methodological Limitations

• Sampling Effects: While sampling rates and data sets were design specific, basic geometric progression can be expanded upon and examined, e.g., exponential and random sampling methods.

- Specificity of Construct: The logic in inverting the Collatz function for purposes here is sound, but other interpretations of the conjecture exist. Exploring these alternate methods could prove insightful.
- Sensitivity of Data: Slight changes to data collection and preparation greatly impact resulting values, leaving tools like correlation analysis accuracy suspect and unusable at this time.
- Restriction of Values: $n \leq 10^7$. Whether the observed properties hold for significantly larger numbers remains an open question. Future research could extend this study by employing parallel computing techniques to analyze a broader numerical range.

6 Conclusion

This study introduced lineage and sibling lineage from the tool set of analogous ancestry and applied it to artifacts of known number systems in analyzing and confirming suspected properties. While its underlying mathematical concept is not new, possibly mundane, and application specific, here it shows potential and aptitude in revealing patterns related to this topic.

Using visual and empirical analysis with scatter and log-log plots and log-log scaling to evaluate Fractal Dimension and Hurst Exponents, the study establishes invariant properties of self-similarity and scaling fractal behaviors in \mathbb{R} for the considered number systems.

Though fractal properties have been established, the near 1.0 value of fractal dimension remains a notable area to explore. An intriguing hypothesis could explore if proximity below the unit mark relates to the topological dimension's D_T placement at zero.

Overall, the results establish significant evidence of scale-invariant properties that adhere to some form of determinism that is neither fully ordered nor fully chaotic. The strong correlation to memory supported by hierarchical empirical output in descendant nodes makes this topic a promising candidate for further quasi-chaotic and complexity studies.

6.1 Future Work - Extended Fractal Dimension Studies

We limited this study's methodology to baseline behavior by focusing on fewer, well-known analytic methods given the uncommon scenario of interest. Certainly, the topic would benefit from RQA, FFT, wavelet, and multi-fractal analysis. Additionally, future work could extend to:

- Further down-tree analysis
- Analogous ancestry examination of level lineage and odd density
- Oscillatory patterns and peak behavior
- Analysis of comparative output by adjusting restrictions on g^{-1}

References

- [1] Wikipedia Contributors. Collatz-tree visualization, 2024. URL https://en.wikipedia.org/wiki/Collatz_conjecture#/media/File: Collatz-tree,_depth=20.svg.
- [2] Thomas H. Cormen, Charles E. Leiserson, and Ronald L. Rivest. *Introduction to Algorithms*. MIT Press, 1990.
- [3] M. G. E. da Luz, D. M. G. dos Santos, E. P. Raposo, and G. M. Viswanathan. Scale-free behavior in hailstone sequences generated by the collatz map. *Phys. Rev. Research*, 3:013073, Jan 2021. URL: https://link.aps.org/doi/10.1103/PhysRevResearch.3.013073, doi:10.1103/PhysRevResearch.3.013073.
- [4] Jeffery P. Dumont and Clifford A. Reiter. Visualizing generalized 3x+1 function dynamics. *Computers and Graphics*, 25:883–898, 2001.
- [5] Craig Alan Feinstein. The collatz 3n+1 conjecture is unprovable, 2011. URL: https://arxiv.org/abs/math/0312309.
- [6] Yukihiro Hashimoto. A fractal set associated with the collatz problem. Bulletin of Aichi University of Education, Natural Science, 56:1–6, 03 2007.
- [7] Clay Mathematics Institute. Millennium prize problems: The riemann hypothesis, 2000. URL: https://www.claymath.org/millennium-problems/riemann-hypothesis.
- [8] Jeffrey C. Lagarias. The 3x+1 problem: An annotated bibliography, ii (2000-2009), 2012. URL: https://arxiv.org/abs/math/0608208.
- [9] Benoit B. Mandelbrot. *The Fractal Geometry of Nature*. W. H. Freeman and Co., 1982.
- [10] T. D. Noe. A127824 triangle in which row n is a sorted list of all numbers having total stopping time n in the collatz (or 3x+1) iteration., 2007. URL: https://oeis.org/A127824.
- [11] Toru Ohira and Hiroshi Watanabe. A conjecture on the collatz-kakutani path length for the mersenne primes, 2012. URL: https://arxiv.org/abs/1104.2804.
- [12] Joseph L. Pe Pe. The 3x+1 fractal. Computers and Graphics, 28:431-435, 2004.
- [13] N. J. A. Sloane. A001511 the ruler function: Exponent of the highest power of 2 dividing 2n. equivalently, the 2-adic valuation of 2n. (formerly m0127 n0051), 2023. URL: https://oeis.org/A001511.
- [14] Eduardo M. K. Souza. Infinity increasing steps on the collatz sequences, 2023. URL: https://arxiv.org/abs/2305.16161.
- [15] X. Wang and X. Yu. Visualizing generalized 3x+1 function dynamics based on fractal. *Applied Mathematics and Computation*, 188:234–243, 03 2007.

- [16] X. Wang and X. Yu. A fractal set associated with the collatz problem. *Progress in Natural Science*, 18:217–223, 03 2008.
- [17] Stephen Wolfram. A New Kind of Science. Wolfram Media, 2002. URL: https://www.wolframscience.com.
- [18] Zach466920. "could this odd insight help explain part of the difficulty in proving the collatz conjecture?". Mathematics Stack Exchange. URL: https://math.stackexchange.com/q/1441208.

A Appendix

A.1 Analogous Ancestry Results and Summary Data

A.1.1 Analogous Ancestry - Extended Topics

Level Lineage: Similar to comparing sibling lineage data but for all nodes on the same level. The motivation comes from adding level 7 to the analysis, where N3 and N21 lineage total to 19 and 18, respectively, yet carry the fractality with other sibling nodes. This could be passive causality driven by their sibligs, something more systemic, or something else. Level lineage would include non-sibling nodes.

Odd Density: The is a mature concept in the Collatz paradigm and was inspired by ideas/graphics from Souza's study of the topic[14]. This would extend lineage of sub-trees to include relative count of odd numbers transvesed by descendant nodes.

A.1.2 Analogous Ancestry - Summary Table Data

Table 5: Summary Analogous Ancestry Data

Node	Number	Tree Level	Lineage	Sibling Lineage	Level Lineage
N5	5	5	9,379,077	93.8%	93.8%
N32	32	5	620,917	6.2%	6.2%
N3	3	7	19	0.0%	0.0%
N20	20	7	9,379,046	100.0%	93.8%
N21	21	7	18	0.0%	0.0%
N128	128	7	$620,\!896$	100.0%	6.2%
N12	12	9	19	_	0.0%
N13	13	9	4,755,822	50.7%	47.6%
N80	80	9	4,623,222	49.2%	46.2%
N84	84	9	16	_	0.0%
N85	85	9	237,641	38.2%	2.4%
N512	512	9	$383,\!252$	61.8%	3.8%
N48	48	11	17	_	0.0%
N52	52	11	4,755,820	_	47.6%
N53	53	11	4,559,258	98.6%	45.6%
N320	320	11	63,961	1.4%	0.6%
N336	336	11	14	_	0.0%
N340	340	11	237,639	_	2.4%
N341	341	11	377,301	98.5%	3.8%
N2048	2048	11	5,948	1.5%	0.1%

Table 6: Basic Statistics for all Nodes by Data Sets: Set Size, Mean, and Standard Deviation (Stnd Dev.)

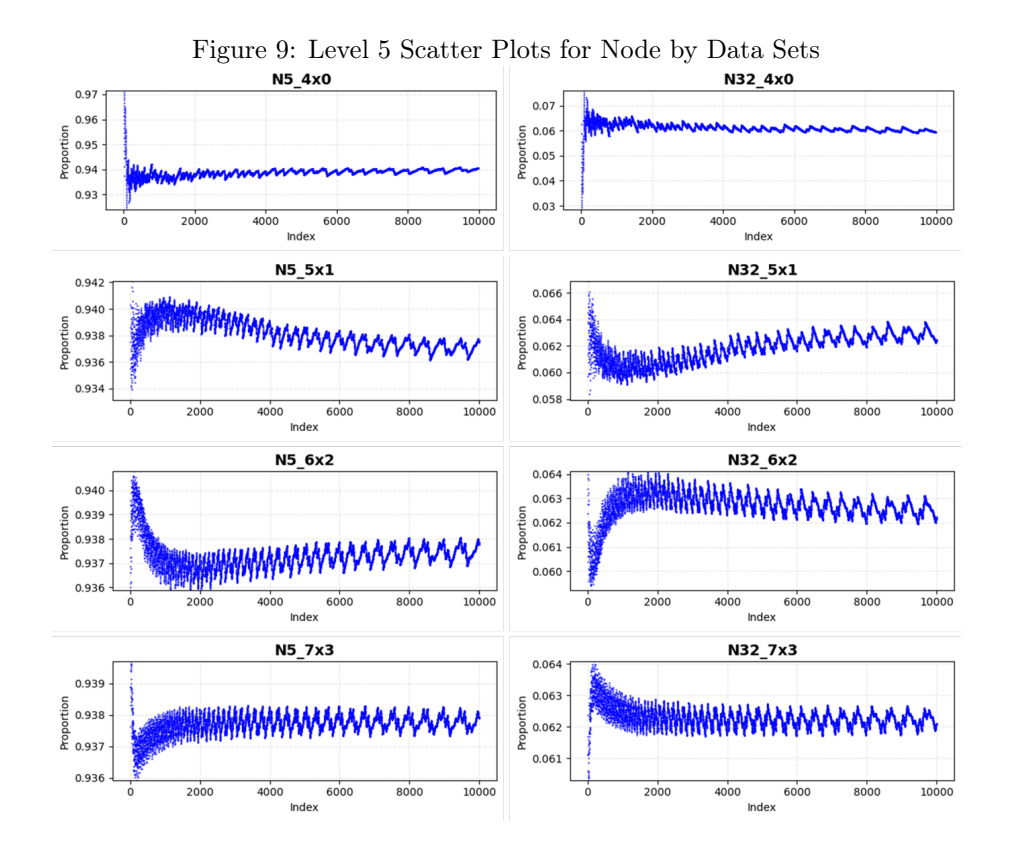
(,0 01100 = 0)	<u>-, </u>		
Data Set	Set Size	Mean	Stnd Dev.
N5 4x0	9984	0.9389	0.0023
N5 5x1	9999	0.9381	0.0013
N5 6x2	9999	0.9373	0.0006
$\frac{\text{N5}}{\text{N5}}$ 7x3	10000	0.9377	0.0003
N32 4x0	9984	0.0611	0.0023
N32_4x0 N32_5x1	9999	0.0611	0.0023
_	9999	0.0619 0.0627	0.0013 0.0006
_			
N32_7x3	10000	0.0623	0.0003
$N3_4x0$	9984	0.0034	0.0061
$N3_5x1$	9999	0.0006	0.0020
$N3_6x2$	9999	0.0001	0.0006
$N3_7x3$	10000	0.0000	0.0001
$N20_4x0$	9984	0.9966	0.0061
$N20_5x1$	9999	0.9994	0.0020
$N20^-6x2$	9999	0.9999	0.0006
$N20^{-}7x3$	10000	1.0000	0.0001
N21 - 4x0	9959	0.0457	0.0784
N21 5x1	9996	0.0083	0.0273
$N21_{-6x2}$	9999	0.0013	0.0079
N21 - 7x3	10000	0.0002	0.0013
N128 4x0	9959	0.9543	0.0013 0.0784
N128_4x0 N128_5x1	9996	0.9943 0.9917	0.0734 0.0273
N128_5x1 N128_6x2	9999	0.9917 0.9987	0.0273 0.0079
N128_6x2 N128 7x3	10000	0.9987 0.9998	0.0079 0.0013
$N13_4x0$	9984	0.4962	0.0242
$N13_5x1$	9999	0.5049	0.0092
$N13_6x2$	9999	0.5066	0.0022
$N13_7x3$	10000	0.5070	0.0007
$N80_4x0$	9984	0.5038	0.0242
$N80_5x1$	9999	0.4951	0.0092
N80 6x2	9999	0.4934	0.0022
N80 7x3	10000	0.4930	0.0007
$N85 \ 4x0$	9926	0.4326	0.0767
N85 5x1	9993	0.4047	0.0267
$N85^{-}6x2$	9999	0.3846	0.0119
N85 7x3	10000	0.3822	0.0028
N512 4x0	9926	0.5674	0.0767
$N512_{-}130$	9993	0.5953	0.0267
N512_6x1 N512_6x2	9999	0.6154	0.0119
N512_0x2 N512_7x3	10000	0.6174	0.00119
N53_4x0	9978	0.9893	0.0018
$N53_{5x1}$	9998	0.9871	0.0011
$N53_6x2$	9999	0.9860	0.0005
$N53_7x3$	10000	0.9861	0.0002
$N320_4x0$	9978	0.0107	0.0018
$N320_5x1$	9998	0.0129	0.0011
$N320_6x2$	9999	0.0140	0.0005
$N320_{-}^{-}7x3$	10000	0.0139	0.0002
N341 - 4x0	9850	0.9822	0.0074
N341 - 5x1	9985	0.9803	0.0026
N341 6x2	9998	0.9831	0.0014
N341 7x3	10000	0.9845	0.0007
N2048 4x0	9850	0.0178	0.0074
N2048_4x0 N2048_5x1	9985	0.0173 0.0197	0.0074
N2048_5x1 N2048_6x2	9998	0.0197 0.0169	0.0020 0.0014
N2048_0x2 N2048_7x3	10000	0.0169 0.0155	0.0014 0.0007
112040_130	10000	0.0100	0.0007

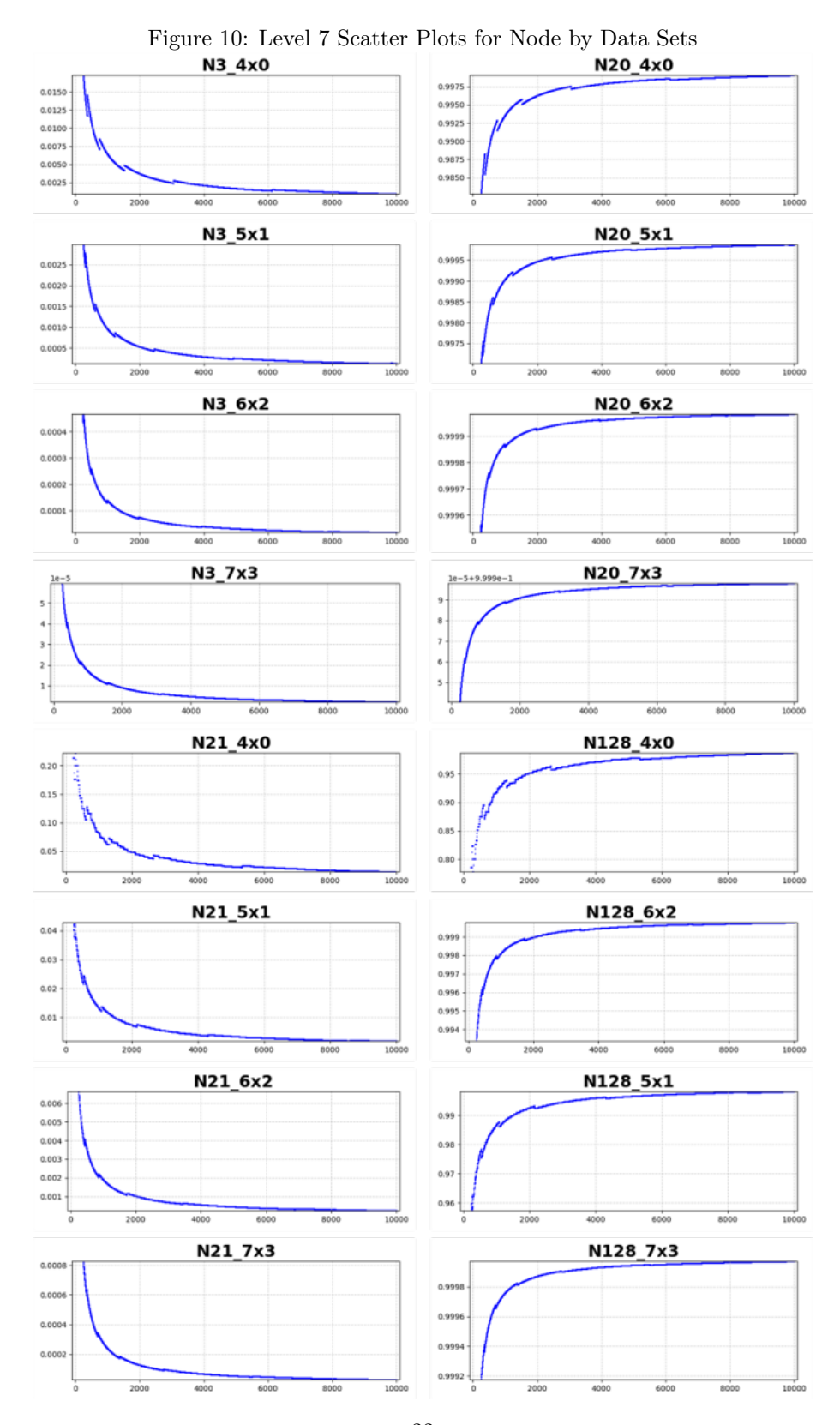
Table 7: Log-Log Analysis Data for Hurst Exponent H (R-Value, P-Value) with Maximum Lag of 100 and Fractal Dimension D (R-Value, P-Value) with Scale 11 for Geometric Box Sequence $(2^i, i \in [0,10])$ for all Nodes by Data Sets.

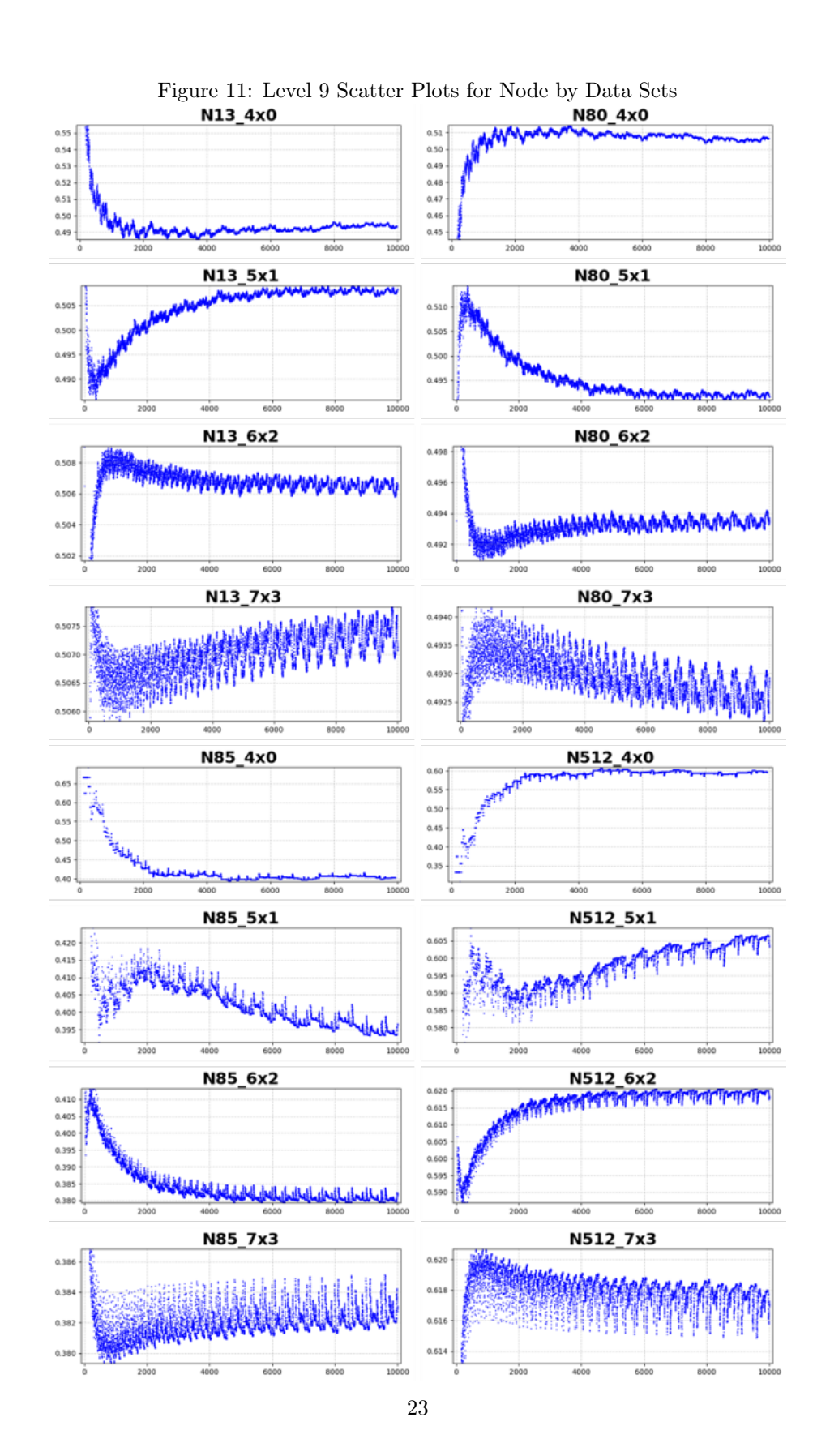
$\begin{array}{c ccccccccccccccccccccccccccccccccccc$	$-Value(D)$ $-25x10^{-23}$ $-34x10^{-25}$ $-39x10^{-25}$ $-25x10^{-23}$ $-34x10^{-25}$ $-34x10^{-25}$ $-34x10^{-25}$
$\begin{array}{c ccccccccccccccccccccccccccccccccccc$	$34x10^{-25}$ $34x10^{-25}$ $39x10^{-25}$ $25x10^{-23}$ $34x10^{-25}$ $34x10^{-25}$
$\begin{array}{c ccccccccccccccccccccccccccccccccccc$	$.34 \times 10^{-25}$ $.39 \times 10^{-25}$ $.25 \times 10^{-23}$ $.34 \times 10^{-25}$ $.34 \times 10^{-25}$
$\begin{array}{c ccccccccccccccccccccccccccccccccccc$	$.39x10^{-25}$ $.25x10^{-23}$ $.34x10^{-25}$ $.34x10^{-25}$
$\begin{array}{c ccccccccccccccccccccccccccccccccccc$	$.25 \times 10^{-23}$ $.34 \times 10^{-25}$ $.34 \times 10^{-25}$
$\begin{array}{c ccccccccccccccccccccccccccccccccccc$	$.34x10^{-25}$ $.34x10^{-25}$
$\begin{array}{c ccccccccccccccccccccccccccccccccccc$	$34x10^{-25}$
$\begin{array}{c ccccccccccccccccccccccccccccccccccc$	
$ \begin{array}{c ccccccccccccccccccccccccccccccccccc$	
$ \begin{array}{c ccccccccccccccccccccccccccccccccccc$	$.39x10^{-25}$
$ \begin{array}{c ccccccccccccccccccccccccccccccccccc$	$.25x10^{-23}$
N3 7x3 0.9941 0.9998 5.37x10 ⁻¹⁶⁹ 0.9959 1.000 2.	$.34x10^{-25}$
$ \begin{array}{c ccccccccccccccccccccccccccccccccccc$	$.34x10^{-25}$
$N20 4x0 = 0.9950 = 0.9998 = 3.6x10^{-109} = 0.9970 = 1.000 = 1.$	$.39x10^{-25}$
160	$.25x10^{-23}$
$N20_5x1$ 0.9939 0.9998 2.35 $x10^{-169}$ 0.9959 1.000 2.	$34x10^{-25}$
	$.34x10^{-25}$
$ \begin{array}{c ccccccccccccccccccccccccccccccccccc$	$.39x10^{-25}$
$ \begin{array}{c ccccccccccccccccccccccccccccccccccc$	$.98 \times 10^{-24}$
$\begin{array}{c ccccccccccccccccccccccccccccccccccc$	$.06x10^{-25}$
	$34x10^{-25}$
	$.39x10^{-25}$
N128_4x0	$.98 \times 10^{-24}$
	0.06×10^{-25}
$N128_{-}6x2$ 0.9737 0.9997 3.76x10 ⁻¹⁵⁸ 0.9959 1.000 2.	$34x10^{-25}$
	$.39x10^{-25}$
	$.25x10^{-23}$
N13_5x1 $\begin{vmatrix} 0.9639 & 0.9998 & 2.03x10^{-168} \\ 0.9959 & 1.000 & 2.03x10^{-168} \\ 0.9959 & 0.9959 & 1.000 & 2.03x10^{-168} \\ 0.9959 & 0.995$	$.34x10^{-25}$
N13_6x2 $\begin{vmatrix} 0.9569 & 0.9998 & 4.78x10^{-165} \\ 0.9959 & 1.000 & 2.8x10^{-165} \\ 0.9959 & 0.9959 & 1.000 & 2.8x10^{-165} \\ 0.9959 & 0.9959 & 0.9959 & 1.000 & 2.8x10^{-165} \\ 0.9959 & 0.9959 & 0.9959 & 0.9959 & 1.000 & 2.8x10^{-165} \\ 0.9959 & 0.9959 & 0.9959 & 0.9959 & 0.9959 & 0.9959 & 0.9959 & 0.9959 \\ 0.9959 & 0.99$	$.34x10^{-25}$
	$.39x10^{-25}$
N80_4x0 0.9763 0.9997 1.86×10^{-157} 0.9970 1.000 1.	$.25x10^{-23}$
	$.34 \times 10^{-25}$
	$34x10^{-25}$
	$39x10^{-25}$
	$.85 \times 10^{-24}$
	$.88 \times 10^{-25}$
	$34x10^{-25}$
$ \begin{array}{c ccccccccccccccccccccccccccccccccccc$	$.39x10^{-25}$
$N512_4x0$ 0.9126 0.9767 5.88x10 ⁻⁶⁶ 0.9959 1.000 7.	$.85 \times 10^{-23}$
$ \begin{array}{c ccccccccccccccccccccccccccccccccccc$	$.88 \times 10^{-25}$ $.34 \times 10^{-25}$
$ \begin{array}{c ccccccccccccccccccccccccccccccccccc$	$.34x10^{-25}$
N53_4x0 0.9823	1.13×10^{-23}
$N53_{5x1} = 0.9767 = 0.9999 = 1.36x10_{-171} = 0.9959 = 1.000 = 2.$	$.23x10^{-25}$
N53_6x2 0.9682	$.34x10^{-25}$
N53_7x3 0.9577 0.9998 $5.10x10^{-168}$ 0.9959 1.000 2.	$.39x10^{-25}$
$N320_{-}4x0$ 0.9858 0.9998 9.63x10 ⁻¹⁶² 0.9969 1.000 1.	$13x10^{-23}$
$ \begin{array}{c ccccccccccccccccccccccccccccccccccc$	$.23x10^{-25}$
$N320_{-}6x2$ 0.9682 0.9999 6.24x10 ⁻¹⁷⁴ 0.9959 1.000 2.	$34x10^{-25}$
$\begin{array}{c ccccccccccccccccccccccccccccccccccc$	$.39 \times 10^{-25}$
	$.59 \times 10^{-22}$
_	$.50 \times 10^{-25}$
	$.23x10^{-25}$
N341_7x3	$.39x10^{-25}$
$N2048_4x0$ 0.9373 0.9748 2.19x10 ⁻⁶⁴ 0.9949 1.000 1.	$.59 \times 10^{-22}$
$N2048_{-5x1}$ 0.9265 0.9963 4.71x10 ⁻¹⁰⁴ 0.9957 1.000 1.	$.50 \times 10^{-25}$
$N2048_{-}6x2 = 0.9613 = 0.9997 = 3.05x10^{-157} = 0.9959 = 1.000 = 2.$	$.23x10^{-25}$
N2048_7x3 0.9685	$.39x10^{-25}$

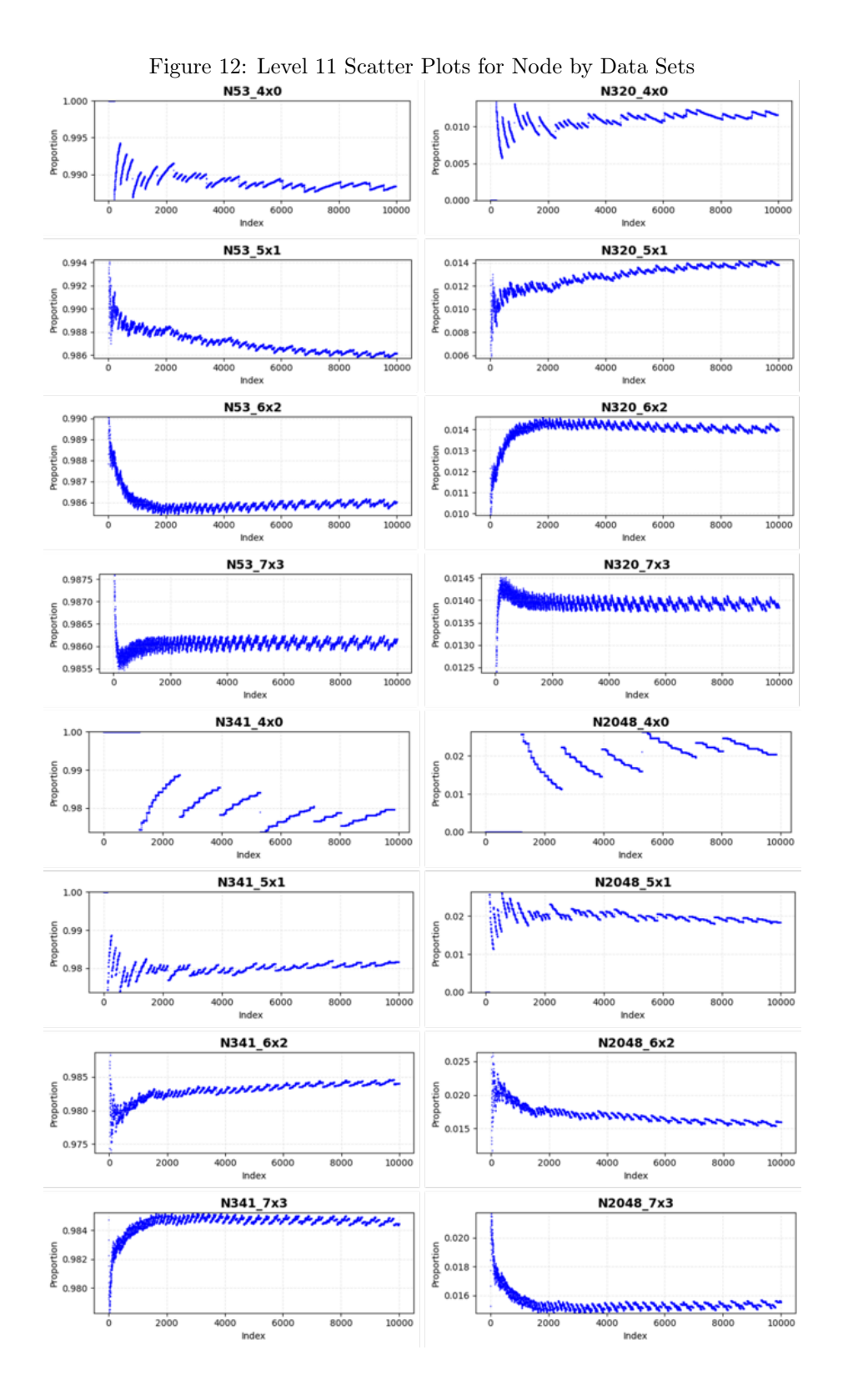
A.2 Visual Data

A.2.1 Scatter Plots for all Nodes By Data Sets









A.3 Fractal Dimension Methods and Exploration Results

Table 8: Box Sequence Test Results For nodes N5, N85, and N320 at sample rates of 4x0 and 7x3: By Row - Normalization in Upper (Z-Score) and Lower (Min/Max) halves, each half separated in thirds for scaling (S9, S11, S13). Column data is in thirds for the three number sequences tested, Geometric (G), Exponential (E), and Psuedo-Linear (PL).

Z-Score	Slope (G)	R-Value	Slope (E)	R-Value	Slope (PL)	R-Value
N5_4x0 (S9)	1.0000	1.0000	0.9914	0.9999	0.9989	1.0000
$N5_{7x3}$	0.9966	1.0000	0.9915	0.9999	0.9993	1.0000
N85 4x0	0.9987	1.0000	0.9960	1.0000	0.9991	1.0000
$N85_7x3$	0.9966	1.0000	0.9915	0.9999	0.9993	1.0000
$N320_4x0$	0.9999	1.0000	0.9913	0.9999	0.9987	1.0000
$\mathrm{N320}_{-}7\mathrm{x3}$	0.9966	1.0000	0.9915	0.9999	0.9993	1.0000
N5_4x0 (S11)	0.9970	1.0000	0.9857	0.9999	0.9988	1.0000
$N5_7x3$	0.9959	1.0000	0.9859	0.9999	0.9982	1.0000
$N85_4x0$	0.9959	1.0000	0.9879	0.9999	0.9988	1.0000
$N85_7x3$	0.9959	1.0000	0.9859	0.9999	0.9982	1.0000
$N320_4x0$	0.9969	1.0000	0.9855	0.9999	0.9986	1.0000
N320_7x3	0.9959	1.0000	0.9859	0.9999	0.9982	1.0000
N5_4x0 (S13)	0.9877	0.9998	0.9754	0.9997	0.9985	1.0000
$N5_7x3$	0.9875	0.9999	0.9757	0.9997	0.9983	1.0000
$N85_4x0$	0.9868	0.9999	0.9764	0.9996	0.9979	1.0000
$N85_7x3$	0.9875	0.9999	0.9757	0.9997	0.9983	1.0000
$N320_4x0$	0.9877	0.9999	0.9753	0.9997	0.9984	1.0000
$\mathrm{N320}_{-}7\mathrm{x3}$	0.9875	0.9999	0.9757	0.9997	0.9983	1.0000
Min/Max	Slope (G)	R-Value	Slope (E)	R-Value	Slope (E)	R-Value
MIII/ Max	biope (G)	rt-varue	Diope (L)	rt-varue	Stope (L)	n-varue
N5_4x0 S(9)	1.0000	1.0000	0.9914	0.9999	0.9988	1.0000
	,				1 . ()	
N5_4x0 S(9)	1.0000	1.0000	0.9914	0.9999	0.9988	1.0000
N5_4x0 S(9) N5_7x3	1.0000 0.9966	1.0000 1.0000	0.9914 0.9915	0.9999 0.9999	0.9988 0.9993	1.0000 1.0000
N5_4x0 S(9) N5_7x3 N85_4x0 N85_7x3 N320_4x0	1.0000 0.9966 0.9979	1.0000 1.0000 1.0000	0.9914 0.9915 0.9955	0.9999 0.9999 1.0000	0.9988 0.9993 0.9982	1.0000 1.0000 1.0000
N5_4x0 S(9) N5_7x3 N85_4x0 N85_7x3	1.0000 0.9966 0.9979 0.9966	1.0000 1.0000 1.0000 1.0000	0.9914 0.9915 0.9955 0.9915	0.9999 0.9999 1.0000 0.9999	0.9988 0.9993 0.9982 0.9993	1.0000 1.0000 1.0000 1.0000
N5_4x0 S(9) N5_7x3 N85_4x0 N85_7x3 N320_4x0	1.0000 0.9966 0.9979 0.9966 0.9972	1.0000 1.0000 1.0000 1.0000 1.0000	0.9914 0.9915 0.9955 0.9915 0.9879	0.9999 0.9999 1.0000 0.9999 0.9999	0.9988 0.9993 0.9982 0.9993 0.9979	1.0000 1.0000 1.0000 1.0000 1.0000
N5_4x0 S(9) N5_7x3 N85_4x0 N85_7x3 N320_4x0 N320_7x3	1.0000 0.9966 0.9979 0.9966 0.9972 0.9966	1.0000 1.0000 1.0000 1.0000 1.0000 1.0000	0.9914 0.9915 0.9955 0.9915 0.9879 0.9915	0.9999 0.9999 1.0000 0.9999 0.9999	0.9988 0.9993 0.9982 0.9993 0.9979 0.9993	1.0000 1.0000 1.0000 1.0000 1.0000 1.0000
N5_4x0 S(9) N5_7x3 N85_4x0 N85_7x3 N320_4x0 N320_7x3 N5_4x0 (S11)	1.0000 0.9966 0.9979 0.9966 0.9972 0.9966	1.0000 1.0000 1.0000 1.0000 1.0000 1.0000	0.9914 0.9915 0.9955 0.9915 0.9879 0.9915	0.9999 0.9999 1.0000 0.9999 0.9999 0.9999	0.9988 0.9993 0.9982 0.9993 0.9979 0.9993	1.0000 1.0000 1.0000 1.0000 1.0000 1.0000
N5_4x0 S(9) N5_7x3 N85_4x0 N85_7x3 N320_4x0 N320_7x3 N5_4x0 (S11) N5_7x3	1.0000 0.9966 0.9979 0.9966 0.9972 0.9966 0.9970 0.9959	1.0000 1.0000 1.0000 1.0000 1.0000 1.0000 1.0000 1.0000	0.9914 0.9915 0.9955 0.9915 0.9879 0.9915 0.9857 0.9859	0.9999 0.9999 1.0000 0.9999 0.9999 0.9999 0.9999	0.9988 0.9993 0.9982 0.9993 0.9979 0.9993 0.9988 0.9982	1.0000 1.0000 1.0000 1.0000 1.0000 1.0000 1.0000 1.0000
N5_4x0 S(9) N5_7x3 N85_4x0 N85_7x3 N320_4x0 N320_7x3 N5_4x0 (S11) N5_7x3 N85_4x0	1.0000 0.9966 0.9979 0.9966 0.9972 0.9966 0.9970 0.9959 0.9953	1.0000 1.0000 1.0000 1.0000 1.0000 1.0000 1.0000 1.0000 1.0000	0.9914 0.9915 0.9955 0.9915 0.9879 0.9915 0.9857 0.9859 0.9875	0.9999 0.9999 1.0000 0.9999 0.9999 0.9999 0.9999 0.9999	0.9988 0.9993 0.9982 0.9993 0.9979 0.9993 0.9988 0.9982 0.9979	1.0000 1.0000 1.0000 1.0000 1.0000 1.0000 1.0000 1.0000 1.0000
N5_4x0 S(9) N5_7x3 N85_4x0 N85_7x3 N320_4x0 N320_7x3 N5_4x0 (S11) N5_7x3 N85_4x0 N85_7x3	1.0000 0.9966 0.9979 0.9966 0.9972 0.9966 0.9970 0.9959 0.9953 0.9959	1.0000 1.0000 1.0000 1.0000 1.0000 1.0000 1.0000 1.0000 1.0000 1.0000	0.9914 0.9915 0.9955 0.9915 0.9879 0.9915 0.9857 0.9859 0.9875 0.9859	0.9999 0.9999 1.0000 0.9999 0.9999 0.9999 0.9999 0.9999 0.9999	0.9988 0.9993 0.9982 0.9993 0.9979 0.9993 0.9988 0.9982 0.9979 0.9981	1.0000 1.0000 1.0000 1.0000 1.0000 1.0000 1.0000 1.0000 1.0000 1.0000
N5_4x0 S(9) N5_7x3 N85_4x0 N85_7x3 N320_4x0 N320_7x3 N5_4x0 (S11) N5_7x3 N85_4x0 N85_7x3 N320_4x0	1.0000 0.9966 0.9979 0.9966 0.9972 0.9966 0.9970 0.9959 0.9953 0.9959 0.9937	1.0000 1.0000 1.0000 1.0000 1.0000 1.0000 1.0000 1.0000 1.0000 1.0000 1.0000	0.9914 0.9915 0.9955 0.9915 0.9879 0.9915 0.9857 0.9859 0.9875 0.9859 0.9821	0.9999 0.9999 1.0000 0.9999 0.9999 0.9999 0.9999 0.9999 0.9999 0.9999	0.9988 0.9993 0.9982 0.9993 0.9979 0.9993 0.9988 0.9982 0.9979 0.9981 0.9972	1.0000 1.0000 1.0000 1.0000 1.0000 1.0000 1.0000 1.0000 1.0000 1.0000 1.0000
N5_4x0 S(9) N5_7x3 N85_4x0 N85_7x3 N320_4x0 N320_7x3 N5_4x0 (S11) N5_7x3 N85_4x0 N85_7x3 N320_4x0 N320_7x3	1.0000 0.9966 0.9979 0.9966 0.9972 0.9966 0.9970 0.9959 0.9953 0.9959 0.9937	1.0000 1.0000 1.0000 1.0000 1.0000 1.0000 1.0000 1.0000 1.0000 1.0000 1.0000	0.9914 0.9915 0.9955 0.9915 0.9879 0.9915 0.9857 0.9859 0.9875 0.9859 0.9821 0.9859	0.9999 0.9999 1.0000 0.9999 0.9999 0.9999 0.9999 0.9999 0.9999 0.9999 0.9999	0.9988 0.9993 0.9982 0.9993 0.9979 0.9993 0.9988 0.9982 0.9979 0.9981 0.9972 0.9982	1.0000 1.0000 1.0000 1.0000 1.0000 1.0000 1.0000 1.0000 1.0000 1.0000 1.0000
N5_4x0 S(9) N5_7x3 N85_4x0 N85_7x3 N320_4x0 N320_7x3 N5_4x0 (S11) N5_7x3 N85_4x0 N85_7x3 N320_4x0 N320_7x3 N5_4x0 (S13)	1.0000 0.9966 0.9979 0.9966 0.9972 0.9966 0.9970 0.9959 0.9953 0.9959 0.9937 0.9959	1.0000 1.0000 1.0000 1.0000 1.0000 1.0000 1.0000 1.0000 1.0000 1.0000 1.0000 0.9998	0.9914 0.9915 0.9955 0.9915 0.9879 0.9915 0.9857 0.9859 0.9875 0.9859 0.9821 0.9859	0.9999 0.9999 1.0000 0.9999 0.9999 0.9999 0.9999 0.9999 0.9999 0.9999 0.9999	0.9988 0.9993 0.9982 0.9993 0.9979 0.9993 0.9988 0.9982 0.9979 0.9981 0.9972 0.9982	1.0000 1.0000 1.0000 1.0000 1.0000 1.0000 1.0000 1.0000 1.0000 1.0000 1.0000 1.0000
N5_4x0 S(9) N5_7x3 N85_4x0 N85_7x3 N320_4x0 N320_7x3 N5_4x0 (S11) N5_7x3 N85_4x0 N85_7x3 N85_4x0 N85_7x3 N320_4x0 N320_7x3 N5_4x0 (S13) N5_7x3	1.0000 0.9966 0.9979 0.9966 0.9972 0.9966 0.9970 0.9959 0.9953 0.9959 0.9937 0.9959	1.0000 1.0000 1.0000 1.0000 1.0000 1.0000 1.0000 1.0000 1.0000 1.0000 1.0000 0.9998 0.9999	0.9914 0.9915 0.9955 0.9915 0.9879 0.9915 0.9857 0.9859 0.9875 0.9859 0.9821 0.9859	0.9999 0.9999 1.0000 0.9999 0.9999 0.9999 0.9999 0.9999 0.9999 0.9999 0.9999 0.9999	0.9988 0.9993 0.9982 0.9993 0.9979 0.9993 0.9988 0.9982 0.9979 0.9981 0.9972 0.9982 0.9985 0.9983	1.0000 1.0000 1.0000 1.0000 1.0000 1.0000 1.0000 1.0000 1.0000 1.0000 1.0000 1.0000 1.0000
N5_4x0 S(9) N5_7x3 N85_4x0 N85_7x3 N320_4x0 N320_7x3 N5_4x0 (S11) N5_7x3 N85_4x0 N85_7x3 N320_4x0 N320_7x3 N5_4x0 (S13) N5_7x3 N5_4x0 (S13) N5_7x3 N5_4x0 (S13)	1.0000 0.9966 0.9979 0.9966 0.9972 0.9966 0.9970 0.9959 0.9953 0.9959 0.9937 0.9959	1.0000 1.0000 1.0000 1.0000 1.0000 1.0000 1.0000 1.0000 1.0000 1.0000 1.0000 0.9998 0.9999 0.9999	0.9914 0.9915 0.9955 0.9915 0.9879 0.9915 0.9857 0.9859 0.9875 0.9859 0.9821 0.9859	0.9999 0.9999 1.0000 0.9999 0.9999 0.9999 0.9999 0.9999 0.9999 0.9999 0.9999 0.9997 0.9997	0.9988 0.9993 0.9982 0.9993 0.9979 0.9993 0.9988 0.9982 0.9979 0.9981 0.9972 0.9982 0.9985 0.9983 0.9971	1.0000 1.0000 1.0000 1.0000 1.0000 1.0000 1.0000 1.0000 1.0000 1.0000 1.0000 1.0000 1.0000 1.0000
N5_4x0 S(9) N5_7x3 N85_4x0 N85_7x3 N320_4x0 N320_7x3 N5_4x0 (S11) N5_7x3 N85_4x0 N85_7x3 N320_4x0 N320_7x3 N5_4x0 (S13) N5_7x3 N5_4x0 (S13) N5_7x3 N5_4x0 (S13) N5_7x3	1.0000 0.9966 0.9979 0.9966 0.9972 0.9966 0.9970 0.9959 0.9953 0.9959 0.9937 0.9959 0.9877 0.9875	1.0000 1.0000 1.0000 1.0000 1.0000 1.0000 1.0000 1.0000 1.0000 1.0000 1.0000 0.9998 0.9999 0.9999	0.9914 0.9915 0.9955 0.9955 0.9915 0.9879 0.9915 0.9857 0.9859 0.9875 0.9859 0.9821 0.9859 0.9754 0.9757 0.9760	0.9999 0.9999 1.0000 0.9999 0.9999 0.9999 0.9999 0.9999 0.9999 0.9999 0.9999 0.9997 0.9997	0.9988 0.9993 0.9982 0.9993 0.9979 0.9993 0.9988 0.9982 0.9979 0.9981 0.9972 0.9982 0.9985 0.9983 0.9971	1.0000 1.0000 1.0000 1.0000 1.0000 1.0000 1.0000 1.0000 1.0000 1.0000 1.0000 1.0000 1.0000 1.0000

Figure 13: Fractal Dimension Levels 5, 7 Log-Log Plots (includes N13). N5_6x2 D=0.9959 r=1.0000 N5_4x0 D=0.9970 r=1.0000 N5_5x1 D=0.9959 r=1.0000 N5_7x3 D=0.9959 r=1.0000 ((a)N)gol ((a)N)Boj -4 -3 log(1/€) -4 -3 log(1/€) -4 -3 log(1/€) → -3 log(1/€) N32_5x1 D=0.9959 r=1.0000 ((a)N)Bol ((a)N)Boj -4 -3 log(1/e) → -3 log(1/e) -4 -3 log(1/€) -4 -3 log(1/e) N3_7x3 D=0.9959 r=1.0000 N3_4x0 D=0.9970 r=1.0000 N3_5x1 D=0.9959 r=1.0000 N3_6x2 D=0.9959 r=1.0000 ((a)N)gol ((a)N)gol -4 -3 log(1/€) → -3 log(1/e) -4 -3 log(1/€) → -3 log(1/€) N20_4x0 D=0.9970 r=1.00 N20_5x1 D=0.9959 r=1.0000 N20_6x2 D=0.9959 r=1.0000 N20_7x3 D=0.9959 r=1.0000 ((a)N)gol log(N(e)) -4 -3 log(1/€) -4 -3 log(1/ε) → -3 log(1/e) $\log(1/\epsilon)$ N21_4x0 D=0.9965 r=1.0000 N21_5x1 D=0.9958 r=1.0000 N21_6x2 D=0.9959 r=1.0000 N21_7x3 D=0.9959 r=1.0000 ((a)N)Bol log(N(e)) -4 -3 log(1/€) -4 -3 log(1/€) -4 -3 log(1/€) -4 -3 log(1/€) N128_5x1 D=0.9958 r=1.0000 N128_4x0 D=0.9965 r=1.0000 N128_6x2 D=0.9959 r=1.0000 N128_7x3 D=0.9959 r=1.0000 ((a)N)gol ((a)N)Bol N13_4x0 D=0.9970 r=1.0000 N13_5x1 D=0.9959 r=1.0000 N13_6x2 D=0.9959 r=1.0000 N13_7x3 D=0.9959 r=1.0000 log(N(e)) log(N(e))

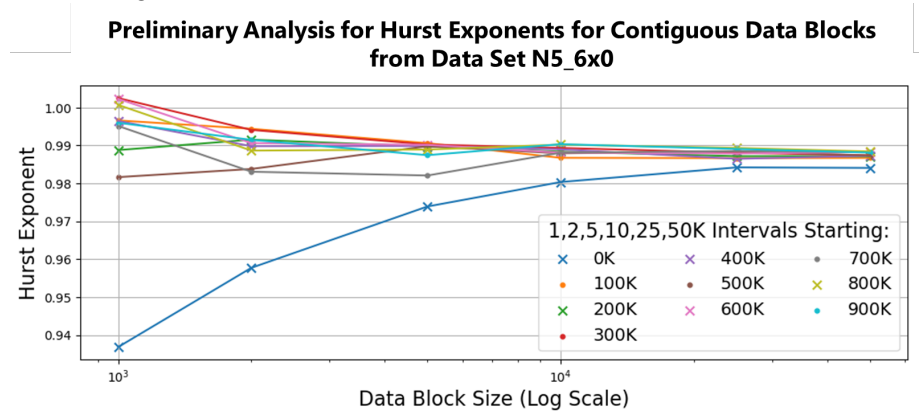
Figure 14: Fractal Dimension Levels 9, 11 Log-Log Plots (excludes N13). N80_5x1 D=0.9959 r=1.0000 N80_6x2 D=0.9959 r=1.0000 N80_7x3 D=0.9959 r=1.0000 ((e)N)Sol ((€)N)Bol -4 -3 log(1/€) -4 -3 log(1/€) -4 -3 log(1/€) -3 −3 log(1/€) N85_4x0 D=0.9959 r=1.0000 log(N(e)) log(N(e)) -4 -3 log(1/€) -3 log(1/e) → -3
log(1/e) → -3
log(1/e) N512_6x2 D=0.9959 r=1.0000 N512_7x3 D=0.9959 r=1.0000 N512_4x0 D=0.9959 r=1.0000 N512_5x1 D=0.9958 r=1.0000 ((a)N)gol ((€))N)Soj -4 -3 log(1/€) → -3 log(1/€) → -3 log(1/€) → -3 log(1/€) N53_4x0 D=0.9969 r=1.0000 N53_5x1 D=0.9959 r=1.0000 N53_6x2 D=0.9959 r=1.0000 N53_7x3 D=0.9959 r=1.0000 log(N(e)) log(N(e)) -4 -3 log(1/€) -4 -3 log(1/€) -4 -3 log(1/€) -4 -3 log(1/€) N320_4x0 D=0.9969 r=1.0000 N320_5x1 D=0.9959 r=1.0000 N320_6x2 D=0.9959 r=1.0000 N320_7x3 D=0.9959 r=1.0000 ((a)N)gol log(N(e)) -4 -3 log(1/€) -4 -3 log(1/€) -4 -3 log(1/€) -4 -3 log(1/€) N341_5x1 D=0.9957 r=1.0000 N341_7x3 D=0.9959 r=1.0000 N341_4x0 D=0.9949 r=1.0000 N341_6x2 D=0.9959 r=1.0000 log(N(e)) log(N(e)) → -3 log(1/€) → -3 log(1/€) N2048_4x0 D=0.9949 r=1.0000 N2048_5x1 D=0.9957 r=1.0000 N2048_6x2 D=0.9959 r=1.0000 N2048_7x3 D=0.9959 r=1.0000 log(N(e)) ((e)N)Sol

A.4 Hurst Exponent Methods and Exploration Results

A.4.1 Data Set Size Preliminary Analysis Using Data Set N5 6x0

Various sized contiguous blocks of data were examined within the span of the first million numbers. We found a certain minimum data set size helped reduce outliers. For a high-level examination, we collected N5 sibling lineage data for the range n=1 to 10^6 , to create data set N5_6x0, and calculated the a Hurst exponent for a range of data blocks (1000, 2000, 5000, 10000, 25000, 50000), starting ever 100K point in the range. The results are in Figure 15 and Table 9. The convergence around 10,000 guided the study's standard set size.

Figure 15: Graphic for preliminary exploratory Hurst exponent analysis: Contiguous data blocks with a maximum lag of 100 at varying length intervals starting every 100K point within a 1M span starting at 1. While informative for determining data set size, later importance included other aspects, such as maximal lag.



A.4.2 Data Set Rescaling Preliminary Analysis Using Various Maximum Lags

We explored maximum lag values of 50, 100, 250, and 500 across all nodes by data sets with the optimal value collecting at 100 as seen in the next graphic. Three sibling pairs have notably similar trends and values (blue outline plots). Four of the nodes (N5, N80, N13, N53) hold the vast majority of lineage and could lead to further study of the factors underlying this data.

Table 9: Data table for preliminary exploratory Hurst exponent analysis for preceding graphic, Figure 15.

Interval	Н	R-Value	Interval	Н	R-Value
1:1001	0.9356	0.9992	500001:501001	0.9804	0.9994
1:2001	0.9569	0.9996	500001:502001	0.9838	0.9997
1:5001	0.9736	0.9998	500001:505001	0.9900	0.9998
1:10001	0.9801	0.9998	500001:510001	0.9875	0.9998
1:25001	0.9840	0.9998	500001:525001	0.9882	0.9998
1:50001	0.9839	0.9998	500001:550001	0.9873	0.9998
100001:101001	0.9947	0.9995	600001:601001	1.0000	0.9991
100001:102001	0.9922	0.9996	600001:602001	0.9898	0.9996
100001:105001	0.9899	0.9998	600001:605001	0.9901	0.9998
100001:110001	0.9867	0.9998	600001:610001	0.9878	0.9998
100001:125001	0.9864	0.9998	600001:625001	0.9876	0.9998
100001:150001	0.9866	0.9998	600001:650001	0.9882	0.9998
200001:201001	0.9888	0.9994	700001:701001	0.9932	0.9993
200001:202001	0.9907	0.9997	700001:702001	0.9811	0.9996
200001:205001	0.9896	0.9998	700001:705001	0.9822	0.9998
200001:210001	0.9883	0.9998	700001:710001	0.9878	0.9998
200001:225001	0.9871	0.9998	700001:725001	0.9883	0.9998
200001:250001	0.9870	0.9998	700001:750001	0.9882	0.9998
300001:301001	1.0019	0.9993	800001:801001	0.9994	0.9991
300001:302001	0.9923	0.9996	800001:802001	0.9892	0.9996
300001:305001	0.9901	0.9997	800001:805001	0.9890	0.9998
300001:310001	0.9891	0.9998	800001:810001	0.9900	0.9998
300001:325001	0.9877	0.9998	800001:825001	0.9891	0.9998
300001:350001	0.9873	0.9998	800001:850001	0.9882	0.9998
400001:401001	0.9969	0.9994	900001:901001	0.9970	0.9995
400001:402001	0.9896	0.9997	900001:902001	0.9912	0.9997
400001:405001	0.9898	0.9998	900001:905001	0.9877	0.9998
400001:410001	0.9890	0.9998	900001:910001	0.9903	0.9998
400001:425001	0.9865	0.9998	900001:925001	0.9890	0.9998
400001:450001	0.9871	0.9998	900001:950001	0.9878	0.9998

Figure 16: Graphic for preliminary exploratory Hurst exponent analysis: Varying maximum lags (x-axis: 50, 100, 250, 500) for all Nodes by Data Sets.

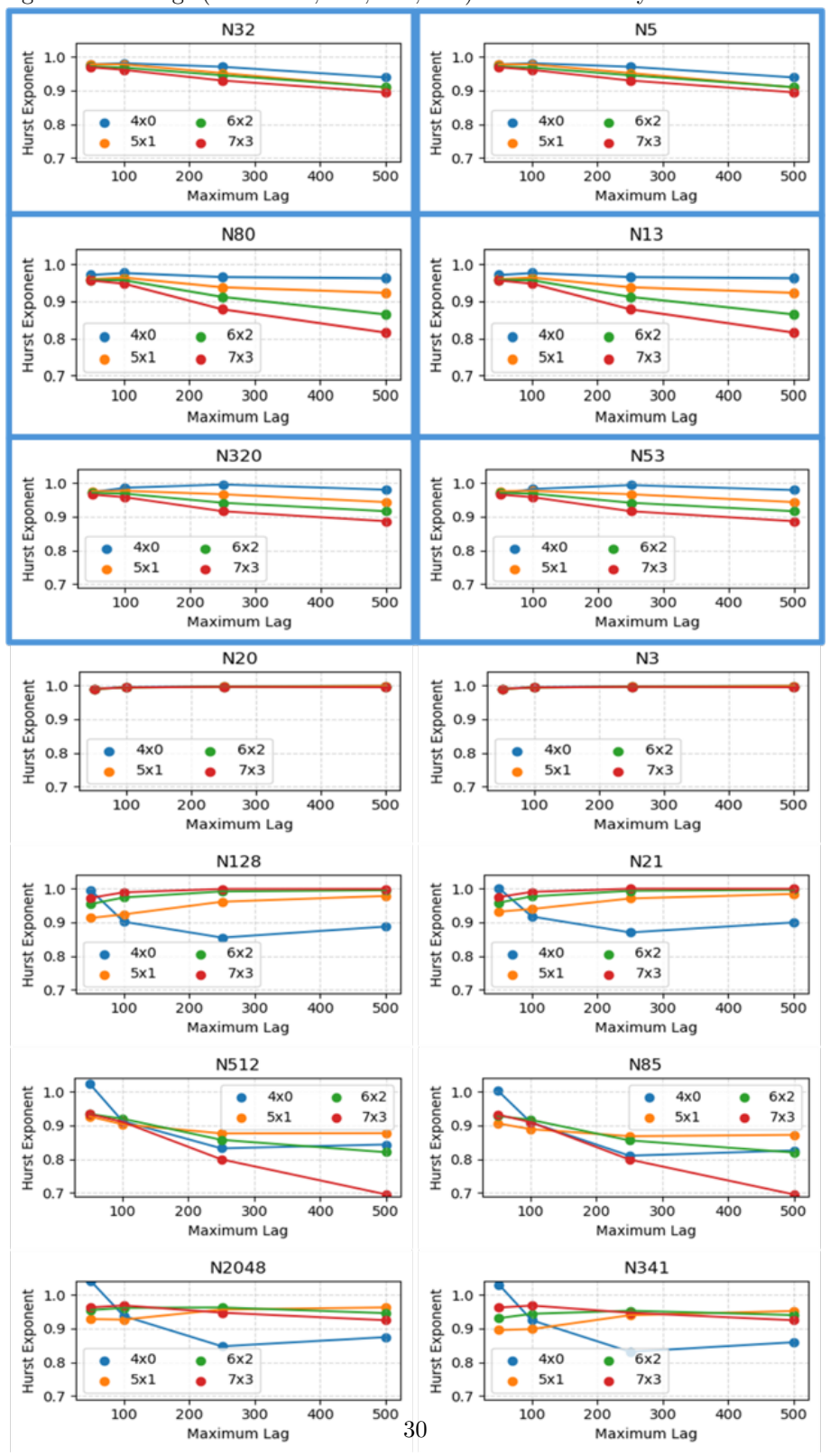


Table 10: Hurst Exponent Analysis Using Various Maximum Lags Across all Nodes by Data Sets [Part 1 of 2]

Data Set	Max. Lag	Н	R-Value	Data Set	Max. Lag	Н	R-Value
$N5_4x0$	50	0.9777	0.9996	N32_4x0	50	0.9777	0.9996
$N5_4x0$	100	0.9810	0.9998	N32_4x0	100	0.9810	0.9998
$N5_4x0$	250	0.9703	0.9998	N32_4x0	250	0.9703	0.9998
$N5_4x0$	500	0.9388	0.9991	N32_4x0	500	0.9388	0.9991
$N5_5x1$	50	0.9777	0.9996	N32_5x1	50	0.9777	0.9996
$N5_5x1$	100	0.9776	0.9998	N32_5x1	100	0.9776	0.9998
$N5_5x1$	250	0.9518	0.9996	N32_5x1	250	0.9518	0.9996
$N5_5x1$	500	0.9090	0.9984	N32_5x1	500	0.9090	0.9984
$N5_6x2$	50	0.9717	0.9997	N32_6x2	50	0.9717	0.9997
$N5_6x2$	100	0.9679	0.9998	N32_6x2	100	0.9679	0.9998
$N5_6x2$	250	0.9451	0.9997	N32_6x2	250	0.9451	0.9997
N5 6x2	500	0.9098	0.9990	N32 6x2	500	0.9098	0.9990
$N5_{7x3}$	50	0.9689	0.9997	N32 7x3	50	0.9689	0.9997
N5 7x3	100	0.9611	0.9998	N32 7x3	100	0.9611	0.9998
N5 - 7x3	250	0.9297	0.9995	N32 7x3	250	0.9297	0.9995
$N5_7x3$	500	0.8946	0.9988	N32_7x3	500	0.8946	0.9988
N3_4x0	50	0.9902	0.9996	N20_4x0	50	0.9901	0.9996
$N3_4x0$	100	0.9950	0.9998	N20_4x0	100	0.9950	0.9998
$N3_4x0$	250	0.9976	0.9999	N20_4x0	250	0.9976	0.9999
$N3_4x0$	500	0.9987	0.9999	N20_4x0	500	0.9987	0.9999
N3 5x1	50	0.9894	0.9996	N20 5x1	50	0.9894	0.9996
N3 5x1	100	0.9939	0.9998	N20 5x1	100	0.9939	0.9998
$\overline{N3}^{-}$ 5x1	250	0.9965	0.9999	N20 5x1	250	0.9965	0.9999
N3 5x1	500	0.9989	0.9999	N20 5x1	500	0.9989	0.9999
$^{-}$ 6x2	50	0.9895	0.9996	N20 6x2	50	0.9895	0.9996
N3 6x2	100	0.9939	0.9998	N20 6x2	100	0.9939	0.9998
N3 6x2	250	0.9962	0.9999	N20 6x2	250	0.9962	0.9999
N3 6x2	500	0.9954	0.9999	N20 6x2	500	0.9954	0.9999
N3 7x3	50	0.9899	0.9996	N20 7x3	50	0.9899	0.9996
N3 7x3	100	0.9941	0.9998	N20 7x3	100	0.9941	0.9998
N3 7x3	250	0.9960	0.9999	N20 7x3	250	0.9960	0.9999
N3 7x3	500	0.9947	0.9999	N20 7x3	500	0.9947	0.9999
N21 4x0	50	1.0007	0.9763	N128_4x0	50	0.9943	0.9798
$N21_{4x0}$	100	0.9170	0.9849	N128 4x0	100	0.9016	0.9856
N21_4x0 N21_4x0	250	0.8699	0.9928	N128 4x0	250	0.8545	0.9929
N21_4x0 N21_4x0	500	0.8996	0.9928 0.9961	N128 4x0	500	0.8872	0.9961
_	500 50			N128_4x0 N128_5x1	500 50	0.8672 0.9129	0.9961 0.9958
N21_5x1		0.9316 0.9394	0.9967	_			
N21_5x1	100		0.9985	N128_5x1	100	0.9234	0.9981
N21_5x1	250	0.9706	0.9992	N128_5x1	250	0.9610	0.9989
N21_5x1	500	0.9841	0.9995	N128_5x1	500	0.9781	0.9993
N21_6x2	50	0.9583	0.9997	N128_6x2	50	0.9544	0.9997
N21_6x2	100	0.9769	0.9997	N128_6x2	100	0.9737	0.9997
N21_6x2	250	0.9933	0.9998	N128_6x2	250	0.9915	0.9998
N21_6x2	500	0.9963	0.9998	N128_6x2	500	0.9952	0.9998
N21_7x3	50	0.9749	0.9997	N128_7x3	50	0.9726	0.9997
N21_7x3	100	0.9902	0.9998	N128_7x3	100	0.9888	0.9998
N21_7x3	250	0.9995	0.9999	N128_7x3	250	0.9989	0.9999
N21_7x3	500	0.9994	0.9999	N128_7x3	500	0.9990	0.9999
N13_4x0	50	0.9707	0.9994	N80_4x0	50	0.9708	0.9994
$N13_4x0$	100	0.9762	0.9997	N80_4x0	100	0.9763	0.9997
$N13_4x0$	250	0.9654	0.9998	N80_4x0	250	0.9654	0.9998
$N13_4x0$	500	0.9621	0.9998	N80_4x0	500	0.9621	0.9998
$N13_5x1$	50	0.9595	0.9997	N80_5x1	50	0.9595	0.9997
$N13_{5x1}$	100	0.9639	0.9998	N80_5x1	100	0.9639	0.9998
N13 $5x1$	250	0.9379	0.9996	N80_5x1	250	0.9379	0.9996

Table 11: Hurst Exponent Analysis Using Various Maximum Lags Across all Nodes by Data Sets [Part 2 of 2]

Data Set	Max. Lag	Н	R-Value	Data Set	Max. Lag	Н	R-Value
$\mathrm{N}13_6\mathrm{x}2$	50	0.9582	0.9997	N80_6x2	50	0.9582	0.9997
$N13_6x2$	100	0.9569	0.9998	N80_6x2	100	0.9569	0.9998
$N13_6x2$	250	0.9119	0.9990	N80_6x2	250	0.9119	0.9990
$N13_6x2$	500	0.8646	0.9979	N80_6x2	500	0.8646	0.9979
$N13_7x3$	50	0.9562	0.9997	N80_7x3	50	0.9562	0.9997
$N13_7x3$	100	0.9476	0.9998	N80_7x3	100	0.9476	0.9998
$N13_7x3$	250	0.8785	0.9977	N80_7x3	250	0.8785	0.9977
$N13_7x3$	500	0.8155	0.9958	N80_7x3	500	0.8155	0.9958
$N85_4x0$	50	1.0037	0.9749	N512_4x0	50	1.0238	0.9705
$N85_4x0$	100	0.9093	0.9825	N512_4x0	100	0.9126	0.9767
$N85_4x0$	250	0.8101	0.9881	N512_4x0	250	0.8320	0.9870
$N85_4x0$	500	0.8257	0.9942	N512_4x0	500	0.8434	0.9937
$N85_5x1$	50	0.9061	0.9954	N512_5x1	50	0.9265	0.9958
$N85_5x1$	100	0.8890	0.9979	N512_5x1	100	0.9034	0.9979
$N85_5x1$	250	0.8680	0.9989	N512_5x1	250	0.8763	0.9988
$N85_5x1$	500	0.8720	0.9991	N512_5x1	500	0.8770	0.9991
$N85_6x2$	50	0.9283	0.9997	N512_6x2	50	0.9337	0.9998
$N85_6x2$	100	0.9166	0.9998	N512_6x2	100	0.9198	0.9998
$N85_6x2$	250	0.8557	0.9977	N512_6x2	250	0.8572	0.9976
$N85_6x2$	500	0.8196	0.9974	N512_6x2	500	0.8205	0.9973
$N85_7x3$	50	0.9321	0.9998	N512_7x3	50	0.9337	0.9998
$N85_7x3$	100	0.9096	0.9996	N512_7x3	100	0.9106	0.9996
$N85_7x3$	250	0.7989	0.9926	N512_7x3	250	0.7993	0.9926
N85_7x3	500	0.6951	0.9856	N512_7x3	500	0.6953	0.9856
$N53_4x0$	50	0.9676	0.9997	N320_4x0	50	0.9730	0.9996
$N53_4x0$	100	0.9823	0.9998	N320_4x0	100	0.9858	0.9998
$N53_4x0$	250	0.9937	0.9998	N320_4x0	250	0.9955	0.9998
$N53_4x0$	500	0.9791	0.9997	N320_4x0	500	0.9801	0.9997
N53_5x1	50	0.9756	0.9997	N320_5x1	50	0.9756	0.9997
N53_5x1	100	0.9767	0.9999	N320_5x1	100	0.9767	0.9999
N53_5x1	250	0.9665	0.9998	N320_5x1	250	0.9665	0.9998
N53_5x1	500	0.9433	0.9994	N320_5x1	500	0.9433	0.9994
N53_6x2	50	0.9707	0.9997	N320_6x2	50	0.9707	0.9997
N53_6x2	100	0.9682	0.9999	N320_6x2	100	0.9682	0.9999
N53_6x2	250	0.9413	0.9996	N320_6x2	250	0.9413	0.9996
N53_6x2	500	0.9163	0.9992	N320_6x2	500	0.9163	0.9992
N53_7x3	50	0.9656	0.9998	N320_7x3	50	0.9656	0.9998
N53_7x3	100	0.9577	0.9998	N320_7x3	100	0.9577	0.9998
N53_7x3	250	0.9161	0.9992	N320_7x3	250	0.9161	0.9992
N53_7x3	500	0.8866	0.9989	N320_7x3	500	0.8866	0.9989
$N341_{-4x0}$	50	1.0300	0.9748	N2048_4x0	50	1.0401	0.9633
$\frac{N341}{4} = \frac{4x0}{4}$	100	0.9245	0.9817	N2048_4x0	100	0.9373	0.9748
N341_4x0	250	0.8310	0.9878	N2048_4x0	250	0.8472	0.9853
$N341_{-4x0}$	500	0.8593	0.9934	N2048_4x0	500	0.8745	0.9924
N341_5x1	50	0.8956	0.9918	N2048_5x1	50	0.9281	0.9916
N341_5x1	100	0.8983	0.9964	N2048_5x1	100	0.9265	0.9963
N341_5x1	250 500	0.9397	0.9982	N2048_5x1	250	0.9565	0.9984
N341_5x1	500	0.9522	0.9989	N2048_5x1	500	0.9626	0.9991
N341_6x2	50	0.9309	0.9991	N2048_6x2	50	0.9551	0.9994
N341_6x2	100	0.9437	0.9995	N2048_6x2	100	0.9613	0.9997
N341_6x2	250	0.9529	0.9998	N2048_6x2	250	0.9625	0.9998
N341_6x2	500	0.9400	0.9994	N2048_6x2	500	0.9457	0.9994
N341_7x3	50	0.9623	0.9997	N2048_7x3	50	0.9628	0.9997
N341_7x3	100	0.9682	0.9998	N2048_7x3	100	0.9685	0.9998
N341_7x3	250	0.9469	0.9997	N2048_7x3	250	0.9470	0.9997
N341_7x3	500	0.9247	0.9994	N2048_7x3	500	0.9247	0.9994